

Climatology, Natural Cycles, and Modes of Interannual Variability of the Great Plains Low-Level Jet as Assimilated by the GEOS-1 Data Analysis System

H. M. Helfand and S. D. Schubert

Data Assimilation Office, Laboratory for Atmospheres
NASA/Goddard Space Flight Center, Greenbelt, Maryland

SUMMARY

Despite huge variations during the course of a typical day, the low-level summertime winds over the southern Great Plains of the United States retain the coherent, jet-like structure of the nighttime hours even after they are averaged over an entire daily cycle. The 15-year mean climatological flow determined numerically by the DAO's GEOS-1 Data Assimilation System agrees well with other types of observations of the low-level jet over the Great Plains (the GPLLJ).

The year-to-year variability of the GPLLJ is much less than its variability during the course of a day, a week, or a month and much weaker than the average flow itself. The year-to-year variability is largest in three places: over eastern Texas to the east and to the south of the place where the flow is strongest, over the western Gulf of Mexico, and over the upper Great Plains (UGP) near the Nebraska and South Dakota.

Much of the variability over Texas comes from an alternating-year fluctuation which occurs only during the first six years of the analysis period. This *intermittent biennial oscillation* (IBO) seems to be dynamically tied to alternating-year fluctuations in local ground wetness and surface temperature during this six-year period. A second pattern of variability, the *continental convergence pattern* (CCP), couples the flow over Texas with that over the UGP. The CCP is revealed only when the IBO is statistically removed from the data set. The CCP also has connections with variability of the North American Monsoon and the flow over the southwestern United States.

The typical duration of the abnormal low-level flow patterns that are responsible for the year-to-year differences grows toward the south over the continent from 2 to 3 weeks over the UGP to 6 to 7 weeks over eastern Texas.

**Climatology, Natural Cycles, and Modes of
Interannual Variability of the Great Plains Low-Level Jet**

H. M. Helfand and S. D. Schubert

Data Assimilation Office, Laboratory for Atmospheres
NASA/Goddard Space Flight Center, Greenbelt, Maryland

ABSTRACT

Despite the fact that the low-level jet of the southern Great Plains (the GPLLJ) of the U. S. is primarily a nocturnal phenomenon that virtually vanishes during the daylight hours, it is one of the most persistent and stable features of the low-level continental flow during the warm-season months, May through August. We have first used significant-level data to validate the skill of the GEOS-1 Data Assimilation System (DAS) in realistically detecting this jet and inferring its structure and evolution. We have then carried out a 15-year reanalysis with the GEOS-1 DAS to determine and validate its climatology and mean diurnal cycle and to study its interannual variability.

Interannual variability of the GPLLJ is much smaller than mean diurnal and random intraseasonal variability and comparable in magnitude, but not location, to mean seasonal variability. There are three maxima of interannual low-level meridional flow variability of the GPLLJ over the upper Great Plains, southeastern Texas, and the western Gulf of Mexico. Cross-sectional profiles of mean southerly wind through the Texas maximum remain relatively stable and recognizable from year to year with only its eastward flank showing significant variability. This variability, however, exhibits a distinct, biennial oscillation during the first six years of the reanalysis period and only then.

Each of the three variability maxima corresponds to a spatially coherent, jet-like pattern of low-level flow interannual variability. There are three prominent modes of interannual variability. These include the *intermittent biennial oscillation (IBO)*, local to the Texas maximum. Its signal is evident in surface pressure, surface temperature, ground wetness and upper air flow, as well. A larger-scale *continental convergence pattern (CCP)* of covariance, exhibiting strong anti-correlation between the flow near the Texas and the upper Great Plains variability maxima, is revealed only when the IBO is removed from the interannual time series. A third, *subtropical mode* of covariance is associated with the Gulf of Mexico variability maximum.

Significant interannual anti-correlations of the southeasterly flow over the Arizona/New Mexico region with the CCP and the subtropical mode are enhanced when restricted to the month of July. These anti-correlations may relate to an observed out-of-phase precipitation relationship between the Great-Plains and the southwestern U. S.

The typical duration of interannual low-level meridional wind anomalies within a given season increases over the continent with decreasing latitude from 2 to 3 weeks over the upper Great Plains to 6 to 7 weeks over eastern Texas.

1. Introduction

Although the low-level jet of the southern Great Plains (GPLLJ) of the U. S. is primarily a nocturnal phenomenon that virtually vanishes during the daylight hours, it is, on longer time scales, one of the most persistent and stable features of the continental low-level flow during the warm-season months, May through August. Bonner (1968) first presented a climatology of the GPLLJ phenomenon by using 2 years of rawinsonde station reports. Bonner and Paegle (1970) further documented the diurnal cycle in the low-level wind at Ft. Worth Tex. from 11 years of data. Whiteman et al. (1997) later pointed out the importance of height and time resolution in observing the LLJ by developing a climatology for north-central Oklahoma based on two years of 8-times-a-day research rawinsonde data.

Mitchell et al. (1995) presented a warm-season (May through August) GPLLJ climatology by using 2 years of hourly observations from the Wind Profiler Demonstration Network. Arritt et al. (1997) later used hourly observations from that same network, now known as the NOAA Wind Profiler Network, to establish a 6-month climatology for the year 1993. They pointed out that the inability of the profiler to make soundings below 500 m might result in the underestimation of LLJ frequency and strength. Anderson and Arritt (2001) extended this data into a seven-year climatology for the summer months June-August for the years 1992-1998.

Helfand and Schubert (1995) carried out a two-month simulation of the springtime GPLLJ with the NASA/DAO GEOS-1 GCM and obtained low-level wind fields with vertical and temporal structures, directionality and climatological distributions that compared favorably with the Bonner climatological data set despite the disparity in the averaging periods. They also examined the role of the GPLLJ in the moisture budget of the United States and found that it transported as much as 1/3 of the moisture that entered the continental U. S., most of it during the night time. What is more important,

they found that the variability of the GPLLJ, largely determined by the variability of its strong night-time phase, is closely tied to the variability of the continental moisture budget. Ghan et al. (1996) found that the ECMWF and NCAR's CCM2 GCMs also simulated the GPLLJ rather well, but with very different spatial distributions.

Higgins et al. (1996) compared assimilations of the springtime GPLLJ in five-year reanalyses with the GEOS-1 and the NCEP/NCAR data assimilation systems and examined the relationship of the LLJ to the assimilated moisture budget in each. In both reanalysis data sets, they found that moisture transport compared favorably with radiosonde observations and that the GPLLJ assimilations captured the basic temporal and structural characteristics documented in previous observational studies. Higgins et al. (1997) carried out a similar comparison of reanalyses for the same five years for the summer months June through August. They found a favorable comparison for the products of both reanalyses with wind profiler data. They also found that the dominant diurnal signal in the Great Plains precipitation during spring and summer is associated with jet events. Anderson and Arritt (2001) found that the NCEP/NCAR reanalysis produced LLJs in a pattern with realistic spatial extent over the central U. S., but with less frequency than observed with the NOAA Wind Profiler Network, with too little extent toward the lee of the Rocky Mountains, and far too few occurrences of strong jets. There was also slightly less interannual variability than observed.

Schubert et al. (1997) used the NASA/DAO GEOS-1 Data Assimilation System (DAS), described in Schubert et al. (1993), to carry out a study to characterize the intraseasonal variability of the moisture flux entering the United States from the Gulf of Mexico. They used a compositing approach to examine how low-level wind maxima on different time scales contribute to moisture transport and how the moisture transport, in turn, interacts with large-scale circulation patterns and precipitation anomalies as functions of time scale.

The current paper extends the GPLLJ intraseasonal variability study of Schubert

et al. (1997) to the interannual time scale. We do not carry out an examination of the variability of moisture transport or precipitation in the current paper but leave that investigation for a future study to be built upon the current results. Section 2 reviews the formulation of the planetary boundary layer (PBL) in the GEOS-1 GCM, validates the ability of the GEOS-1 DAS to capture the evolution and structure of the GPLLJ and discusses the DAS integration that has been carried out for this study. Section 3 presents the mean diurnal and seasonal cycles and the mean warm-season climatology of the GPLLJ for the 15-year assimilation and compares the climatology to independent observations. It also examines interannual variability of the GPLLJ in the context of intraseasonal variability. In section 4 we examine year-to-year persistence and stability of the GPLLJ and discuss a biennial oscillation that occurs only during the first 6 years of the reanalysis. Section 5 investigates the spatial coherence of interannual anomalies of the GPLLJ and delineates characteristic modes of these anomalies. It also investigates anti-correlation of these modes with the flow over the southwestern United States. In section 6, we examine the temporal coherence and intraseasonal duration of interannual anomalies of the GPLLJ. We summarize our results in section 7.

2. Formulation and validation of the planetary boundary layer and integration of the GEOS-1 DAS

a. Formulation of the planetary boundary layer parameterization

The vertical structure of the planetary boundary layer (PBL) is explicitly resolved in the GEOS-1 GCM, which drives the GEOS-1 DAS, into a region of several model layers that should approximate the physical depth of the PBL. A 100 hPa deep PBL, for example, would consist of 4 model layers. Turbulent vertical fluxes of momentum, heat

and moisture either within the PBL or in disjoint layers of turbulence above it are parameterized by the level 2.5, second-order turbulence closure scheme of Helfand and Labraga (1988). The bottom half of the lowest layer of the GCM corresponds to an atmospheric surface layer for which wind, temperature and humidity profiles and the turbulent surface fluxes of heat, moisture, and momentum are modeled by Monin-Obukov similarity theory. The Appendix of Helfand and Schubert (1995) further discusses the level 2.5 turbulence parameterization and surface-layer schemes.

b. Validation of the PBL parameterization

The value of a skillful atmospheric data assimilation system is that it can use the atmospheric data that is available to infer additional information that is not directly accessible. Determination of the vertical structure of the PBL is an excellent example of such inferred information. Conventional atmospheric soundings at mandatory levels such as 1000 hPa and 850 hPa miss the entire structure of the PBL and cannot therefore detect the existence of the nocturnal LLJ, so prevalent over the Great Plains. Thus the assimilated low-level flow structure must be largely driven by the physics of the PBL parameterization.

We have obtained extra significant-level data to verify the skillfulness of the GEOS-1 DAS in creating a time series (Fig. 1) of the structure of the lower atmosphere near Ft. Worth, Texas for the month of August 1993. The extra significant-level data was not used in the assimilation. Comparison of the assimilation (denoted by the colored shading in the figure) with a separate analysis that incorporated the extra significant-level data but not the DAS (denoted by the contours in the figure) indicates a faithful reproduction of the diurnal periodicity of low-level wind speeds by the DAS and a reasonable representation of day-to-day variability in the strength and vertical structure of

the nocturnal jet. Note, for example, the lack of a nocturnal jet in both the assimilation and the significant-level analysis for the mornings of August 3, 4, 27, and 28 as well as the enhanced strength and depth of the assimilated and the analyzed jets for August 6 and 23. This comparison validates the skill of the GEOS-1 DAS and its PBL parameterization to realistically infer the structure and evolution of the GPLLJ and provides confidence to carry out an assimilation experiment for the study of the GPLLJ and its variability.

c. Integration of the GEOS-1 DAS

The GEOS-1 DAS (Schubert et al., 1993) was integrated for the 15 year period, 1980 through 1994, at a resolution of 2^0 latitude by 2.5^0 longitude with 20 σ -pressure levels in the vertical. These include 5 levels below 800 hPa and 7 levels above 200 hPa. Boundary conditions were taken from observations of sea-surface temperature and off-line computations of soil moisture carried out with a simple bucket model from monthly mean observed surface air temperature and precipitation data (Schemm et al., 1992). All fields were saved every six simulated hours at mandatory pressure levels and at the model σ -levels to minimize both the errors and the loss of information introduced by interpolation and sampling. This is particularly important for resolving the low-level jet, which is confined to the lowest kilometer and has a strong diurnal component.

3. Climatology and natural variability of the GPLLJ

a. The mean diurnal cycle of the GPLLJ

The low-level flow over the continental United States exhibits significant variability over a number of different time scales, in the GEOS-1 15-year reanalysis data set, from the diurnal to the multi-annual. These variations include regular diurnal and seasonal cycles and irregular fluctuations on all time scales. The mean diurnal cycle has been computed by taking the 1845-day average of jet frequency and winds for 15 warm seasons (May-August) at each of four synoptic times (Fig. 2). This cycle is strongest over the southern Great Plains, where Bonner criterion-1 jets (wind speed maximum $\geq 12 \text{ m s}^{-1}$, with a decrease of at least 6 m s^{-1} , see Bonner, 1968) occur at least 50% of the time during the nocturnal hours over an elongated region from northern Mexico to the Oklahoma Panhandle and then disappear during the daytime. Peak values reach as high as 70% at 0600 UTC (or 0000 LST) and 60% at 1200 UTC (0600 LST), at which time the region begins to contract. Low-level ($\sigma = .97$, approximately 250 m above the ground) winds accelerate and rotate clockwise during the night to peak southerly values of 11 m s^{-1} in the Texas Panhandle (at 0600 UTC) and in the Big Bend region (at 1200 UTC) and then nearly vanish over the continent by local noontime (0600 UTC) each day.

Curiously, a pair of jet maxima also appears in the low-level northerly flow over the eastern Pacific Ocean just off the continental coast. They exhibit weaker diurnal signals than the GPLLJ because they occur over ocean. Helfand and Schubert (1995) have seen these jets in simulations with the GEOS-1 GCM and have discussed possible observational evidence for them. Additional observational evidence for the northern California jet has been presented by Beardsley et al. (1987), Zemba and Friehe (1987), Dorman et al. (1999), and Parish (2000).

b. The mean climatology of the GPLLJ

Despite the large daily excursions, the seasonal mean flow over the southern Great Plains takes on the coherent character of the nocturnal jet-like structure, but with weaker amplitude. The mean low-level southerly wind reaches a maximum of about 7.4 m s^{-1} (Fig. 3a) over west-central Texas. Mean criterion-1 jet frequency (Fig. 3b) exceeds 30% in a curved region connecting a series of relative maxima at the northeast corner of the Texas Panhandle, near the Big Bend of the Rio Grande, and just south of the Mexican border and west of Brownsville, Texas (not indicated with the present contour interval). The Northern California Jet is as also quite evident in the time mean, while the Baja California Jet is less distinct.

This assimilated Great Plains frequency pattern for the warm season is weaker than that obtained by Helfand and Schubert (1995) in their 2-month LLJ simulation, and it is a narrower and more extended pattern with multiple relative maxima. The assimilated jet off the California coast is also located further to the north. This pattern is in better agreement with the original Bonner (1968) 2-year, 12-month climatology, with its north, northeastward leaning axis, its 30% maximum near the Texas and Oklahoma Panhandles, and its secondary maximum near Brownsville Texas, than was the 2-month simulation by Helfand and Schubert (1995).

Comparison of seven years (1992-1998) of nocturnal wind profiler observations for June through August (Anderson and Arritt, 2001, Fig. 2), with the 15-year climatology for that period (Fig. 4) suggests a high bias for the reanalysis of about 15% in the central Great Plains (between about 32° and 44°N), even in the lee of the Rockies, at 0600 UTC and an even higher bias over western Kansas and the Texas and Oklahoma Panhandles at 1200 UTC, but with a contraction of the frequency peak toward the southern Great Plains, as occurs in the observations. However, the profiler observations are subject to a low bias because they cannot see wind maxima that occur below 500 m (Arritt et al.,

1997). Whiteman et al. (1997) found, in fact, that Bonner criterion-1 LLJs occurred about 50% of the time at both 0500 UTC and 1100 UTC (see their Fig. 3a) during two warm seasons over the ARM SGP CART site near the Nebraska border (denoted by the "X"s in our Fig. 4), in excellent agreement with the current results.

c. Variability due to the mean diurnal and seasonal cycles of the GPLLJ

The mean seasonal cycle for the warm season, obtained by taking 15-year averages for each of the four months of the warm season (Fig. 5), varies less dramatically in the Great Plains region than does the diurnal cycle, but still quite significantly. Peak low-level southerly winds increase noticeably from 5.9 m s^{-1} in May to 8.5 m s^{-1} in June and July and then decrease slightly to 7.0 m s^{-1} in August. The maximum shifts slightly westward and northward from May to August as the zone of southerlies narrows and elongates. Maximal jet frequencies increase from 31% in May to 37% in July and then decrease again in August, with a continuous shift in the position and a split into two separate peaks by August.

The amplitude of the mean diurnal cycle, defined as the standard deviation of departures at the four synoptic times from the 15-year mean, take on their largest values (Figs. 6a and c) in the central to southern Great Plains and in eastern Mexico, nearly coincident with the mean field maxima of the GPLLJ. These standard deviations range from about half as large as the magnitudes of the mean fields themselves to slightly larger.

The similarly defined amplitude of the mean seasonal cycle is considerably weaker over the GPLLJ region than that for the diurnal cycle: only about 30% as strong for meridional wind (Fig. 6b) and only about 25% as strong for jet frequency (Fig. 6d). The maxima are located in the subtropics, at the flanks of the mean jet pattern, with the

maximum for meridional wind speed extending into the mid-continent. These maxima seem to reflect the contraction from the Gulf of Mexico of the GPLLJ and its western expansion as the season progresses.

d. Comparison of interannual variability with regular and random intraseasonal variability

At this point, we will focus on natural, irregular fluctuations of the low-level southerly wind only and not on those of LLJ frequency because wind strength varies more smoothly in time and space and in amplitude, and because it is a better measure of the transport of moisture and will therefore be important to our future investigation of the LLJ's contribution to the variability of the moisture budget over the central U. S.

Standard deviations on the synoptic time scale (periods more than a day and up to 8 days; see Appendix A for the computation of the standard deviations of this section) have a maximum over the northern Great Plains near the South Dakota/Nebraska border (Fig. 7a), where the mean meridional wind field is small. As the time scale of the random fluctuations increases to the super-synoptic (periods more than 8 days and up to a month, with the mean seasonal cycle removed, Fig. 7b) to the seasonal (periods more than a month and up to a season, with the mean seasonal cycle removed, Fig. 7c; note the change in contour interval) to interannual (the standard deviation of the seasonal means, Fig. 7d), the peaks of these fluctuations advance due southward over the Great Plains to Nebraska/Kansas, Oklahoma, and then Texas and the Gulf of Mexico and their amplitudes decrease noticeably, reflecting a change of character from extratropical, weather-related changes in flow pattern to slower, subtropical adjustments to the mean climatology.

Note that there are three maxima of interannual variability of the GPLLJ: a 1.1 m s^{-1} peak over southeastern Texas, to the east and south of the mean velocity peak, a 1.0 m s^{-1} peak over the western Gulf of Mexico, and a $.9 \text{ m s}^{-1}$ peak in the upper Great Plains (UGP) near the Nebraska/South Dakota border. We shall see in a later section of this paper that the typical period of coherence of a climate anomaly increases over the continent from 2 to 3 weeks over the UGP to 6 to 7 weeks over eastern Texas.

Standard deviations of the interannual variability of the GPLLJ (Fig. 7d) are small compared to the magnitudes of the mean fields themselves and compared to diurnal and synoptic-scale fluctuations. Peak standard deviations are only about 15% as large as peak values of the mean field itself. Local values of this ratio range from about 10% to 25% over the southern Great Plains and northeastern Mexico. The interannual standard deviations of the GPLLJ compare in magnitude, but not in geographical location, to those of the mean seasonal cycle: the interannual variations are largest precisely in the gaps between the seasonal maxima, a few degrees to the east and to the south of the GPLLJ. Random, non-cyclical fluctuations on the seasonal time scale (Fig. 7c) are slightly larger than the interannual variations and are more nearly collocated.

4. Year-to-year stability of the meridional flow and the *intermittent biennial oscillation*

a. Year-to-year stability

Because interannual variability of the GPLLJ is so relatively small, its structure is quite persistent from year to year, as can be seen for example, in the zonal cross sections of seasonally averaged, low-level meridional wind at 30°N , the latitude where the largest variability peak occurs, in Fig. 8a. A pronounced jet structure consistently occurs during

each year of the 15-year reanalysis in the vicinity of 102.5°W . The meridional velocity peak occasionally becomes displaced one or two degrees eastward, but the structure of the jet is stable and easily recognizable in each year of the data set. The profile to the west of the peak is surprisingly consistent from year to year with a maximal spread from minimum to maximum of only about 30% of the mean value. The eastward flank of the jet can vary in spread by 75% of the mean value or, alternatively, it can vary in width by a factor of as large as two.

The 15 cross sections have been repeated, 5 or 6 at a time, for better visibility in Figs. 8b-d with the same sequence of line types, weights, and markings and labeled by year. Notice a marked biennial oscillation of the profiles during the first six years (1980-85) of the data set (Fig. 8b) between 95°W and 97.5°W which fades into slower and weaker 3- to 4-year fluctuations after the seventh year of the reanalysis data set.

b. The intermittent biennial oscillation

The geographic distribution of the magnitude of the detrended biennial oscillation for the first six years of the reanalysis (see Appendix B) is presented in Fig. 9a. This *intermittent biennial oscillation* (IBO) is confined to a narrow band over eastern Texas between about 95°W and 97.5°W and to an equally narrow band to the north of Texas between Arkansas and eastern Oklahoma. The IBO is largest between 28°N and 30°N , near the southeastern Texas peak of variability, where the detrended average difference between the "even" years and the "odd" years reaches nearly 3 m s^{-1} . The oscillation decreases rapidly both to the north and to the south, becoming barely noticeable by about 42°N to the north and by about 22°N to the south. (An IBO is noticeable over the western Gulf, however, for a shorter, four-year period of intermittency, 1980-83, but oscillations in the time series in this region then reverse phase from 1983 to 1985.)

The IBO over eastern Texas is related to biennial oscillations from 1980 to 1985 in ground wetness (not shown) and in surface temperature (Fig. 9b) over south central Texas. There appears to be a clear dynamical relationship between the IBO in low-level flow over eastern Texas and oscillations over south central Texas of surface temperature (T_g), ground wetness, and surface pressure. Subnormal ground wetness in the region during the "even" years leads to reduced latent cooling of the ground. This results in warm surface temperatures and in a narrow, shallow low in surface pressure (Fig. 9c) directly above the temperature anomaly. Together with a broad high off the Gulf coast, the low drives a southerly jet during the "even" years over the flatter terrain to its east. This relationship between soil moisture, evaporation, and jet strength is similar to that found in numerical simulations by Paegle et al. (1996) and Bosilovich and Sun (1999).

The IBO signal remains coherent all the way up to the 200 hPa level (Fig. 9d), where the low-level southerly jet over eastern Texas merges with a weaker surface jet over Arizona to form the poleward branch of an upper level anticyclonic gyre that covers half of the continental U. S. This 200 hPa jet extends from the Gulf of California to the Canadian border.

Interannual variability over Texas is dominated by the IBO. Over 2/3 of the variance over eastern Texas is directly due to the mean biennial oscillation of the first six years of the reanalysis period so that only 55% of the standard deviation of interannual variability variance remains there after this oscillation has been removed and the relative maximum disappears from that location. Interannual standard deviations over most other regions, including the relative maxima over the UGP and the Gulf of Mexico, remain virtually unchanged.

c. Verification of the intermittent biennial oscillation in other data sets

Fig. 5b (the thin line) of a paper by Hu and Feng (2000) shows an obvious biennial oscillation during the summer months June-August for the years 1979-86 in the time series for a sea-level pressure gradient index that measures the low-level meridional flow near the Texas reference point. It is interesting that the biennial nature of this oscillation disappears at slightly higher elevations. (The thin line of Fig. 5a shows an index for the average of the 850 hPa and the 925 hPa flows.) The IBO for the warm-season months for the years 1979 through 1986 can also be seen in the 925 hPa meridional winds in the NCEP/NCAR reanalysis data set, even though the $\sigma = .97$ winds in the GEOS-1 product and the 925 hPa winds in the NCEP/NCAR product are evaluated at different heights above the ground. The IBO can be seen as well in the NCEP/NCAR 200 hPa heights and winds.

5. Spatial coherence of GPLLJ variability

a. Spatial covariances

The characteristics of the flow in the proximity of the interannual variability maxima over the UGP, Texas, and the Gulf of Mexico can be further analyzed by looking at patterns of spatial coherence. Interannual covariances have been computed between meridional winds at reference points (42°N , 97.5°W ; 30°N , 97.5°W ; and 22°N , 95°W ; respectively) for each of the three maxima and wind components at all grid points in the domain. The covariances, shown in Fig. 10a-c as contours for the meridional wind component and as wind vectors, have been normalized by dividing by the interannual

standard deviation of meridional wind for the relevant reference point to obtain units of velocity.

A local, spatially coherent, jet-like pattern of approximately 10^0 width and 10^0 to 15^0 length dominates the covariance pattern for each reference point. The dark (light) shading indicates the 99% (95%) confidence interval, based on the use of the Fisher z-transform (see von Storch and Zwiers, 1999, p. 148), for pointwise correlation of the meridional flow with the reference point. Interannual covariances with the UGP and Gulf of Mexico points define continental-scale patterns including significant anti-correlations with one another (at the 95% confidence level) and significant correlations (up to the 99% confidence level) with the flow along the Texas coast and that over the region of the North American Monsoon System (NAMS). In addition, both points have noticeable covariances with the meridional flows off the coasts of northern and Baja California and with the zonal flows over the Mexican Plateau, the southeastern U. S., and the adjacent Atlantic Ocean. The UGP point has significant anti-correlations, as well, over Louisiana, Florida, and the Midwest while the Gulf point exhibits noticeable covariances with the flows over the northern Gulf of Mexico, the Texas Panhandle, the Northwest, and east of the subtropical Pacific High.

On the other hand, only very limited nonlocal features appear in the pattern for the Texas reference point, including a weak anti-correlation (northerly covariances) with the flow near the UGP point, weak westerly covariances over the Mexican Plateau, the Rocky Mountains, the Ohio River Valley, the southeastern U. S. and adjacent Atlantic Ocean, and a weak easterly covariance over the southern Gulf of Mexico. This covariance pattern highly resembles the IBO shown in Fig. 9a over the southern Great Plains but does not share the features of the IBO in the western U. S. or off the Pacific coast.

b. Removal of the IBO

The normalized interannual covariances of low-level meridional flow with the Texas reference point change dramatically (Figs. 10e) when one applies a filter that removes the mean of the biennial oscillation for 1980-85 from the first six years of all time series (see Appendix B). This removal of the IBO reveals a continental-scale covariance pattern with decreased, but still highly significant (at the 99% level), covariances over Texas and the surrounding area. The covariance maximum shifts incrementally to the east. Covariances over the UGP become intensified (they are even stronger than covariances over the reference point), broader, and significant to the 99% level. Significant meridional wind covariances also become revealed over the western Gulf of Mexico, the NAMS region, the Midwest, and the Pacific Northwest.

Interannual covariances for the UGP reference point (Fig. 10d), on the other hand, are largely unaffected by removal of the IBO except over eastern Texas, where the confidence level reaches 99%. The covariance maximum in this region shifts toward, but does not quite reach, the Texas reference point.

The pattern of covariances with the Texas point nearly matches that with the UGP point over most of the continent and even over the western Gulf of Mexico except, of course, for a reversal of phase. The striking similarity of this pair of patterns suggests that short-term, local disturbances, such as the IBO, mask a natural pattern of interannual variability over the continent.

Interannual covariances with the Gulf of Mexico reference point (Fig. 10f) remain mostly unchanged except for a slight increase in magnitude and significance over eastern Texas.

c. Covariances with surface pressure

It is perhaps easier to visualize the similarity of the interannual-minus-IBO covariance patterns for the UGP and the Texas points by looking at patterns of normalized surface pressure covariance with those points (Figs. 10g and h). These two patterns have nearly identical features, but with opposite phase: a sharp, narrow high (low) sits over the northern Great Plains and a broad high (low) over the Gulf of Mexico, while a nearly continent-wide trough (ridge) connects lows (highs) over Texas/New Mexico and Great Lakes. This trough (ridge) helps to divide the low-level continental-scale flow into a convergent (divergent) pattern of northerlies (southerlies) in the northern Great Plains and southerlies (northerlies) over eastern Texas and the western Gulf of Mexico. We will thus designate this common pattern of covariance for the UGP and Texas reference points as the *continental convergence pattern* (CCP). The low (high) over Texas/New Mexico helps to explain the anti-correlation between southerly flow over eastern Texas and southeasterly flow over Arizona/New Mexico.

The pattern of interannual-minus-IBO surface-pressure covariance with the Gulf of Mexico point (Fig. 10i) is generally similar to that for the UGP point (but with opposite phase) in that it is dominated by a Rocky Mountain low along an axis from southern Texas to northern Idaho adjacent to highs over the northern Great Plains and the Gulf of Mexico. The Rockies low, however, is more elongated and displaced northward over northern Utah. The Gulf of Mexico high is stronger and more zonally-symmetric, extending into Baja California and the Pacific Ocean. The high in the northern Great Plains is deeper and broader, and the low over the Great Lakes is absent so there is little sense of continental-scale convergence. This covariance pattern is clearly quite distinct from the CCP or the IBO pattern. Because it is more clearly defined over the subtropics south of about 32°N , we will designate this third pattern as the *subtropical mode of*

covariance, even though it also exhibits important covariances over the northern tier of the U. S.

d. Anti-correlation with the flow over southwestern U. S.

The interannual anti-correlation between low-level flow over Arizona/New Mexico and that over lower Great Plains in the CCP and subtropical modes may very well correspond to an out-of-phase interannual correlation, established by Higgins et al. (1998), between the seasonally-averaged precipitation in the southwestern U. S. and that over the Great Plains. Hu and Feng (2000) have shown a strong linkage between interannual fluctuations in the strength of the GPLLJ and in summertime precipitation over the central U. S., and Carleton (1986), Douglas (1995), and Stensrud et al. (1995) suggest that a relationship may exist between the strength of the Gulf of California LLJ and southwest monsoon precipitation. While the 2^0 by 2.5^0 grid of the GEOS-1 DAS cannot properly resolve the Gulf of California, the significant (up to the 99% confidence level) interannual anti-correlation between southeasterly flow along the western slopes of the southern Rockies with the southerly flow over the lower Great Plains suggests an out-of-phase dynamical relationship related to the observed out-of-phase precipitation relationship.

Because the southwest monsoon does not begin until mid way through the warm season, around the beginning of July, we have also calculated normalized interannual covariance of *monthly* anomalies of low-level flow with the Texas reference point (Fig. 11). We have found somewhat stronger anti-correlations for the month of July than for seasonal anomalies (and statistically significant at the 99% confidence level) over both the NAMS region and the UGP but no significant covariances for any other month. Results for the other two reference points are similar except that the Gulf point also has

significant anti-correlations over the NAMS and UGP regions (at the 95% confidence level) for the month of June.

6. Duration and temporal coherence of interannual anomalies

The interannual climatological anomalies do not persist uniformly throughout an entire season, but fluctuate from month to month and even from week to week. To estimate characteristic temporal scales of coherence and spatial structures for these fluctuations, we examine the lag covariance of weekly anomalies of low-level wind from the mean seasonal cycle with southerly anomalies at the three reference points. These lag covariances have been computed over the entire 15-year period of the data set and have been normalized by dividing by the standard deviation of the weekly anomaly at the reference point. The lag-covariance vectors are shown in Figs. 12-14 for time lags ranging from minus 4 weeks to plus 4 weeks. Contours are shown only for the meridional wind component, and statistical significance for the meridional component is indicated by the 95% (and 99%) confidence levels in the light (and dark) shading.

The zero-lag weekly covariance patterns (Figs. 12e, 13e, and 14e) are locally similar to those for season-long anomalies, but with magnitudes two and a half to three times as large and with broader regions of significant correlation. There is little mutual flow covariance between pairs of the reference points at zero lag. The Texas and Gulf points, however, exhibit significant covariance with the westerly to northwesterly flow over the Mexican Plateau and over the southwestern U. S. This relationship is similar to that for interannual anomalies and may relate in the same way to an observed (Mo et al., 1997; Higgins et al., 1997; and Mo, 2000) inverse intraseasonal rainfall relationship between the southwestern U. S. and the Great Plains.

Covariances diminish significantly for all three points from zero lag to a lag of plus or minus one week. Local covariances with the UGP point become statistically

insignificant by a lag of plus or minus two weeks, indicating that the largest local anomalies there have a coherence time scale of only 2 to 3 weeks. Local covariances with the other two reference points remain significant for longer times; covariances with the Texas point remain significant through a lag of plus or minus three weeks, indicating a coherence time scale of 6 to 7 weeks, while those with the Gulf point maintain their significance for plus or minus two weeks, indicating a coherence time scale of 4 to 5 weeks.

Local covariances for the latter two reference points do not always decrease monotonically with increasing time. Local covariance with the Texas point increases substantially from a lag of plus (minus) two weeks to a lag of plus (minus) three weeks, and then it suddenly vanishes. This may be the result of a continental-scale feedback between southerly (northerly) anomalies over Texas and northerly (southerly) anomalies over the upper Great Plains region where the flow over the UGP responds to that over Texas with a two-week delay (Fig. 12d or 13g). The flow over Texas responds in turn to that over the UGP with an additional one-week delay (Fig. 12f or 13d) to give an additional southerly acceleration of the flow over Texas after a net delay of three weeks. This three-week resurgence of correlation might also relate to a 22-day oscillation observed by Mo (2000) in summertime precipitation and flow patterns over the continental U. S.

An even more substantial increase in local meridional covariance occurs with the Gulf point from a lag of plus (minus) one week to a lag of plus (minus) two weeks. This is followed by a gradual diminution of the anomaly with increasing lag. The two-week resurgence of southerly anomalies over the Gulf seems to relate to a two-week oscillation in the strength of westerly anomalies over the Mexican Plateau and its impact on the anticyclonic turning of the mean southeasterly flow over the western Gulf of Mexico.

7. Summary

Significant-level data has helped us to validate the ability of the of the GEOS-1 DAS and its PBL parameterization to represent and therefore to assimilate the structure and variability of the GPLLJ. We have therefore had the confidence to carry out a 15-year reanalysis with the GEOS-1 DAS to determine the jet's climatology and mean diurnal cycle and to study its interannual variability in the context of shorter-term variability.

Despite huge diurnal variations, the mean climatological low-level flow over the southern Great Plains exhibits a persistent, coherent structure similar to that of the nocturnal jet. The mean climatology of the reanalysis is in good general agreement both with the original two-year rawinsonde climatology of Bonner (1968) and with the more recent seven-year, nocturnal wind-profiler climatology of Anderson and Arritt (2001), especially in light of the documentation of the low bias of the wind-profiler data set. There are also significant low-level, northerly jets, in the GEOS-1 reanalysis, off the coasts of upper and Baja California. Natural variability of the GPLLJ tends to decrease in magnitude and shift equatorward as the period of these variations increases from the synoptic to the super-synoptic to the random seasonal to the interannual time scale. The typical duration of an interannual anomaly within a given season also increases over the continent with decreasing latitude from 2 to 3 weeks over the upper Great Plains to 6 to 7 weeks over eastern Texas.

The GPLLJ is a very stable long-term feature of the Great Plains and adjacent Gulf of Mexico during the warm season. Its three interannual variance maxima are small relative to mean diurnal variance and to the mean fields themselves and are comparable in magnitude but not in structure or location to mean seasonal variance. The largest of the three maxima is located over eastern Texas slightly to the east and to the south of the mean-flow maximum, and the other two, slightly weaker maxima are located over the western Gulf of Mexico and in the upper Great Plains near the Nebraska/South Dakota

border. Cross-sectional profiles of mean southerly wind over central Texas repeat a stable and easily recognizable structure from year to year in this region with significant fluctuations only to the east of the velocity maximum.

This variability, however, exhibits a distinct, biennial oscillation for the first six years of the reanalysis period. The NCEP/NCAR reanalysis data set and work by Hu and Feng (2000) seem to indicate that this IBO may even extend to the 8-year period 1979-1986. This low-level intermittent biennial signal is fairly well localized to the southern Great Plains, but it grows with height into an anticyclonic gyre that, by the 200 hPa level, covers half of the continental U. S. A 200 hPa southerly jet extends from the Gulf of California to the Canadian border. This structure is also observed in the NCEP/NCAR reanalysis data set.

There appears to be a clear dynamical relationship between the IBO mode over eastern Texas and oscillations of T_g , ground wetness and surface pressure over south central Texas. Subnormal ground wetness leads to reduced latent cooling of the ground resulting in warm surface temperatures, giving rise to a narrow, shallow pressure low which drives an anticyclonic flow featuring a southerly jet to the flatter terrain to its east.

Patterns of interannual covariance with the meridional flow at three reference points centered over the three maxima of interannual variability of the low-level meridional wind reveal three primary modes of coherent interannual fluctuation. These including the IBO, a larger-scale *continental convergence pattern*, which is masked by the IBO unless it is removed from the interannual time series, and a third, mostly *subtropical mode* associated with the western Gulf of Mexico reference point.

Statistically significant interannual anti-correlation of the southeasterly flow over Arizona/New Mexico with the LLJ, present in the CCP and subtropical modes, perhaps reflects interannual anti-correlation between the GPLLJ and the Gulf of California and an observed interannual anti-correlation between precipitation in the southwestern U. S. and that over the Great Plains observed by Higgins et al. (1998). This low-level flow anti-

correlation is very evident for interannual climatological anomalies restricted to the month of July and for intraseasonal anomalies on the weekly time scale as well.

Acknowledgments.

We wish to thank Chung-Yu (John) Wu for preparation of the data in Grads format and the plotting of Fig. 1. This work was supported by the Global Modeling and Analysis Program of the NASA Earth Sciences Enterprise.

APPENDIX A

Computation of Intraseasonal Variances

The daily variance $V_{\text{daily},j}$ for the j th week (8-day period) is

$$V_{\text{daily},j} = [\sum_i (U_{i,j} - U_{\text{week},j})^2] / 8 = (\sum_i U_{i,j}^2) / 8 - U_{\text{week},j}^2, \quad (\text{A.1})$$

where $U_{i,j}$ is the daily average for the i th day of the j th week of the variable U , $U_{\text{week},j}$ is the weekly average for the j th week, and the summation \sum_i is over the daily index i . The synoptic-scale variance is simply taken as the mean weekly variance for the 240 weeks of the entire 15-year period or

$$\begin{aligned} V_{\text{synop}} &= (\sum_j V_{\text{daily},j}) / 240 \\ &= \{ \sum_j [\sum_i (U_{i,j} - U_{\text{week},j})^2] / 8 \} / 240 \\ &= \{ \sum_j [\sum_i U_{i,j}^2] / 8 \} / 240 - (\sum_j U_{\text{week},j}^2) / 240 \\ &= (\sum_{i,j} U_{i,j}^2) / (8 \times 240) - (\sum_j U_{\text{week},j}^2) / 240. \end{aligned} \quad (\text{A.2})$$

This can be rewritten as

$$\begin{aligned} V_{\text{synop}} &= [(\sum_{i,j} U_{i,j}^2) / (8 \times 240) - U_{\text{clim}}^2] - [(\sum_j U_{\text{week},j}^2) / 240 - U_{\text{clim}}^2]. \\ &= V_{\text{daily}} - V_{\text{weekly}}, \end{aligned} \quad (\text{A.3})$$

where U_{clim} is the climatological mean value of the variable U over the entire 15-year period of the reanalysis, where the summation \sum_j is over the monthly index j , where the summation $\sum_{i,j}$ is over both the daily index i and the monthly index j , and where V_{daily} and V_{weekly} are the total daily and the total weekly variances, respectively, of the variable U about the 15-year mean U_{clim} .

Similarly, the supersynoptic and seasonal variances can be written as

$$\begin{aligned} V_{\text{supersyn}} &= [(\sum_j U_{\text{week},j}^2) / 240 - U_{\text{clim}}^2] - [(\sum_k U_{\text{month},k}^2) / 60 - U_{\text{clim}}^2]. \\ &= V_{\text{weekly}} - V_{\text{monthly}}, \end{aligned} \quad (\text{A.4})$$

and

$$\begin{aligned} V_{\text{seasonal}} &= [(\sum_k U_{\text{month},k}^2) / 60 - U_{\text{clim}}^2] - [(\sum_l U_{\text{year},l}^2) / 15 - U_{\text{clim}}^2]. \\ &= V_{\text{monthly}} - V_{\text{interannual}}, \end{aligned} \quad (\text{A.5})$$

where V_{monthly} and $V_{\text{interannual}}$ are the total monthly and the interannual (season-long) variances, respectively, of the variable U about the 15-year mean U_{clim} , where $U_{\text{month},k}$ is the monthly average for the k th month, where $U_{\text{year},l}$ is the seasonal average for the l th year, and the summations \sum_k and \sum_l are over the monthly and annual indices k and l , respectively. The random supersynoptic and seasonal variances, shown as standard deviations in Fig. 7, are the same as (A.4) and (A.5) except that the variance due to the mean 15-year climatological seasonal cycle is subtracted out from V_{weekly} and V_{monthly} . Thus,

$$V_{\text{rand supersyn}} = V_{\text{rand weekly}} - V_{\text{rand monthly}}, \quad (\text{A.6})$$

and

$$V_{\text{rand seasonal}} = V_{\text{rand monthly}} - V_{\text{interannual}}, \quad (\text{A.7})$$

where

$$V_{\text{rand weekly}} = [(\sum_j U_{\text{week},j}^2) / 240] - [(\sum_k U_{\text{clim week},k}^2) / 16] \quad (\text{A.8})$$

and

$$V_{\text{rand monthly}} = [(\sum_k U_{\text{month},k}^2) / 60] - [(\sum_l U_{\text{clim month},l}^2) / 4]. \quad (\text{A.9})$$

Here $U_{\text{clim week},k}$ and $U_{\text{clim month},l}$ are the mean values of U averaged over the k th week of all 15 years and the l th month of all 15 years, respectively, of the reanalysis data set.

APPENDIX B

Computation of the Intermittent Biennial Oscillation (IBO)

The mean deviation (or signed amplitude) of the intermittent biennial oscillation for the time series U_{year} for the six-year period 1980-85 can be naively defined as:

$$U_{IBO} = (1/6) \times (U_{1980} + U_{1982} + U_{1984} - U_{1981} - U_{1983} - U_{1985}) / 6 \quad (\text{B.1})$$

Suppose, however, that the mean slope per year, U_{slope} , of the time series during that period is non-trivial, and that the variable U_{year} therefore has a mean linear trend,

$$T_{\text{year}} = U_{\text{slope}} \times (\text{year} - 1982.5). \quad (\text{B.2})$$

According to (B.1), the linear trend T_{year} possesses a biennial oscillation of mean deviation

$$T_{IBO} = (T_{1980} + T_{1982} + T_{1984} - T_{1981} - T_{1983} - T_{1985}) / 6 = -3 U_{\text{slope}} / 6, \quad (\text{B.3})$$

even though it by itself shows absolutely no oscillatory behavior. Thus only a portion of the mean deviation U_{IBO} diagnosed in (B1) truly represents the IBO. It is necessary therefore to detrend the time series U_{year} before determining the true amplitude of its IBO.

To detrend the time series U_{year} , we write

$$D_{\text{year}} = U_{\text{year}} - T_{\text{year}}, \quad (\text{B.4})$$

where T_{year} is defined in (B.2) and where we have chosen to set

$$\begin{aligned} U_{slope} &= (U_{1984.5} - U_{1980.5}) / 4. \\ &= ((U_{1984} + U_{1985}) - (U_{1980} + U_{1981})) / 8, \end{aligned} \quad (B.5)$$

to ensure that the slope of the filtered time series is identical to that of the original one

U_{year} .

The mean deviation of the detrended time series is

$$\begin{aligned} U^D_{IBO} &= (D_{1980} + D_{1982} + D_{1984} - D_{1981} - D_{1983} - D_{1985}) / 6 \\ &= (U_{1980} + U_{1982} + U_{1984} - U_{1981} - U_{1983} - U_{1985}) / 6 \\ &\quad - (T_{1980} + T_{1982} + T_{1984} - T_{1981} - T_{1983} - T_{1985}) / 6 \\ &= U_{IBO} - T_{IBO} \\ &= U_{IBO} - U_{slope} / 2. \end{aligned} \quad (B.6)$$

The filtered time series with the IBO removed is the set of equations:

$$U^B_{1980} = U_{1980} - U^D_{IBO} \quad (B.7)$$

$$U^B_{1981} = U_{1981} + U^D_{IBO}$$

$$U^B_{1982} = U_{1982} - U^D_{IBO}$$

$$U^B_{1983} = U_{1983} + U^D_{IBO}$$

$$U^B_{1984} = U_{1984} - U^D_{IBO}$$

$$U^B_{1985} = U_{1985} + U^D_{IBO}$$

$$U^B_{1986} = U_{1986}$$

$$U^B_{1987} = U_{1987}$$

etc.

Indeed, we see that the slope for the filtered time series U^B_{year} is

$$\begin{aligned}
 U^B_{\text{slope}} &= ((U^B_{1984} + U^B_{1985}) - (U^B_{1980} + U^B_{1981})) / 8 \\
 &= ((U_{1984} + U_{1985}) - (U_{1980} + U_{1981})) / 8 \\
 &= U_{\text{slope}} .
 \end{aligned}
 \tag{B.8}$$

REFERENCES

- Anderson, C. J., and R. W. Arritt, 2001: Representation of summertime low-level-jets in the central United States by the NCEP/NCAR reanalysis. *J. Climate*, **14**, 234-247.
- Arritt, R. W., T. D. Rink, M. Segal, D. P. Todey, C. A. Clark, M. J. Mitchell, and K. Labas, 1997: The Great Plains low-level jet during the warm-season of 1993. *Mon. Wea. Rev.*, **125**, 2176-2192.
- Beardsley, R., C. E. Dorman, C. A. Friehe, L. K. Rosenfeld, and C. D. Winant, 1987: Local atmospheric forcing during the Coastal Ocean Dynamics Experiment. 1. A description of the marine boundary layer and atmospheric conditions over a northern California upwelling region. *J. Geophys. Res.*, **92**, 1467-1488.
- Bonner, W. D., 1968: Climatology of the low level jet. *Mon. Wea. Rev.*, **96**, 833-850.
- _____, and J. Paegle, 1970: Diurnal variations in the boundary layer winds over the south central United States in summer. *Mon. Wea. Rev.*, **98**, 735-744.
- Bosilovich, M. G., and W.-Y. Sun, 1999: Numerical simulation of the 1993 midwestern flood: land-atmosphere interactions. *J. Climate*, **12**, 1490-1505.
- Carleton, A. M. 1986: Synoptic-dynamic character of "bursts" and "breaks" in the southwest U. S. summer precipitation singularity. *J. Climatol.* **5**, 389-402.
- Dorman, C. E., D. P. Rogers, W. Nuss, and W. T. Thompson, 1999: Adjustment of the summer marine boundary layer around Point Sur, California. *Mon. Wea. Rev.*, **127**, 261-282.
- Douglas, M. W., 1995: The summertime low-level jet over the Gulf of California. *Mon. Wea. Rev.*, **123**, 2334-2347.
- Ghan, S. J., X. Bian, and L. Corsetti, 1996: Simulation of the Great Plains low-level jet and associated clouds by general circulation models. *Mon. Wea. Rev.*, **124**, 1388-1408.

- Helfand, H. M., and J. C. Labraga, 1988: Design of a non-singular level 2.5 second-order closure model for the prediction of atmospheric turbulence. *J. Atmos. Sci.*, **45**, 113-132.
- _____, and S. D. Schubert, 1995: Climatology of the Great Plains low-level jet and its contribution to the continental moisture budget of the United States. *J. Climate*, **8**, 784-806.
- Higgins, R. W., K. C. Mo, and S. D. Schubert, 1996: The moisture budget of the central United States in spring as evaluated in the NCEP/NCAR and the NASA/DAO reanalyses. *Mon. Wea. Rev.*, **124**, 939-963.
- _____, E. S. Yao, E. S. Yarosh, J. E. Janowiak, and K. C. Mo 1997: Influence of the Great Plains low-level jet on summertime precipitation and moisture transport over the central United States. *J. Climate*, **10**, 481-507.
- _____, K. C. Mo, and E. S. Yao 1998: Interannual variability of the U. S. summer precipitation regime with emphasis on the southwestern monsoon. *J. Climate*, **11**, 2582-2606.
- Hu, Q., and S. Feng, 2001: Climatic role of southerly flow from the Gulf of Mexico in interannual variations in summer rainfall in the central United States. *J. Climate*, **14**, 3156-3170.
- Mitchell, M. J., R. W. Arritt, and K. Labas, 1995: A climatology of the warm-season Great Plains low-level jet using wind profiler observations. *Weath. and Forecast.*, **10**, 576-591.
- Mo, K. C., 2000: Intraseasonal modulation of summer precipitation over North America. *Mon. Wea. Rev.*, **128**, 1490-1505.
- _____, J. N. Paegle, and R. W. Higgins, 1997: Atmospheric processes associated with summer floods and droughts in the central United States. *J. Climate*, **10**, 3028-3046.

- Paegle, J., K. C. Mo, and J. Nogues-Paegle, 1996: Dependence of simulated precipitation on surface evaporation during the 1993 United States summer floods. *Mon. Wea. Rev.*, **124**, 345-361.
- Parish, T. R., 2000: Forcing of the summertime low-level-jet along the California coast. *J. Appl. Meteor.*, **39**, 2421-2433.
- Schemm, J.-K., S. Schubert, J. Terry, S. Bloom and Y. Sud, 1992: Estimates of monthly mean soil moisture for 1979-89, *NASA Tech. Memo. 104571*, 252 pp.
- Schubert, S. D., R. B. Rood, and J. Pfaendtner. 1993: An assimilated dataset for earth-science applications. *Bull. Amer. Meteor. Soc.*, **74**, 2331-2342.
- _____, H. M. Helfand, C.-Y. Wu, and W. Min, 1998: Subseasonal variations in warm-season moisture transport and precipitation and moisture transport over the central and eastern United States. *J. Climate*, **11**, 2530-2555.
- Stensrud, D. J., R. L. Gall, S. L. Mullen, and K. W. Howard, 1995: Model climatology of the Mexican Monsoon. *J. Climate*, **8**, 1775-1794.
- von Storch, H. and F. W. Zwiers, 1999: *Statistical Analysis In Climate Research*. Cambridge University Press, 484 pp.
- Whiteman, C. D., X. D. Bian, and S. Y. Zhong, 1997: Low-level jet climatology from enhanced rawinsonde observations at a site in the southern Great Plains. *J. Appl Meteor.*, **36**, 1363-1376.
- Zemba, J., and, C. A. Friehe, 1987: The summer marine atmospheric boundary layer jet in the Coastal Ocean Dynamics Experiment. *J. Geophys. Res.*, **92**, 1489-1496.

FIGURE CAPTIONS

Figure 1. Time series of GPLLJ wind-speed profiles over Ft. Worth, Texas for August 1993 for an assimilation carried out with the GEOS-1 DAS with conventional data only (colored shading) and for a second validation analysis using both conventional and significant-level wind data but not the DAS (the contour lines).

Figure 2. The mean diurnal cycle of low-level ($\sigma = .97$, about 250 m above the surface) meridional velocity (contours of 1 m s^{-1} , the zero contour is omitted), wind vectors (reference arrow = 10 m s^{-1}), and Bonner criterion-1 jet frequency (per cent, shaded). The cycle is averaged over the 15 warm seasons (May-August) of the GEOS-1 15-Year Reanalysis Data Set. Local times are a) 1800 CST, b) 0000 CST, (contours of 2 m s^{-1}), c) 0600 CST (contours of 2 m s^{-1}), and d) 1200 CST, (contours of 1 m s^{-1}), approximately 6 hours earlier than the UTC times.

Figure 3. a) The 15-year, warm-season mean low-level wind vectors (reference arrow = 10 m s^{-1}) and low-level meridional velocity (contours of 1 m s^{-1} , the zero contour is omitted) and b) wind vectors and Bonner criterion-1 jet frequency (contours of 5 per cent) assimilated by the GEOS-1 Reanalysis Data Set.

Figure 4. The 15-year, summertime (June-August) mean Bonner criterion-1 jet frequency (contours of 10 per cent) and low-level wind vectors (reference arrow = 10 m s^{-1}) assimilated by the GEOS-1 Reanalysis Data Set over the region of the NOAA Wind Profiler Network for a) 0600 UTC and b) 1200 UTC. The "X"s near the Oklahoma/Nebraska border denote the location of the ARM SGP CART site where Whiteman et al (1997) observed about 50% frequency of Bonner criterion-1 jets at both 0500 UTC and 1100 UTC.

Figure 5. The mean seasonal cycle of low-level meridional velocity (contours of 1 m s^{-1} , the zero contour is omitted), wind vectors (reference arrow = 10 m s^{-1}), and Bonner criterion-1 jet frequency (per cent, shaded) during the warm season May-August. The cycle is averaged over the 15-year period of the GEOS-1 Reanalysis Data Set.

Figure 6. Standard deviation of the mean diurnal cycle of Fig. 2 (panels a and c), and the mean seasonal cycle of Fig. 4 (panels b and d). Low-level meridional wind (shaded, contour interval $.25, .15 \text{ m s}^{-1}$) is shown in panels a and b and Bonner criterion 1 jet frequency (shaded, contour interval 5, 2 per cent) is shown in panels c and d. These are superimposed over the 15-year, warm-season mean low-level wind vectors (reference arrow = 10 m s^{-1}).

Figure 7. Standard deviation of low-level meridional velocity (shaded, contour interval $.5 \text{ m s}^{-1}$) associated with natural, random variability on a) the synoptic time scale (more than a day and up to 8 days), b) the super-synoptic time scale (more than 8 days and up to a month, with the mean seasonal cycle removed, with an extra dashed contour for 2.75 m s^{-1}), c) the seasonal time scale (more than a month and up to a season, with the mean seasonal cycle removed, contour interval $.25 \text{ m s}^{-1}$), and d) the interannual time scale (warm-season averages, contour interval $.1 \text{ m s}^{-1}$ with an extra dashed contour for 0.9 m s^{-1}). Vectors are mean low-level flow (reference arrow = 10 m s^{-1}).

Figure 8. Cross-sections of the mean low-level meridional velocity (ms^{-1}) at 30°N latitude a) for each of the 15 warm seasons of the GEOS-1 Reanalysis Data Set with the interannual standard deviation in the gray line with triangles and b-d) repeated, 5 or 6 at a time, with the same sequence of colors, line styles (solid, dashed, or dotted), and line markings (no markings, open circles or closed squares) and labeled by year. Notice the marked biennial oscillation of the profiles during the first 6 years (1980-85) of the data set (panel b).

Figure 9. The intermittent biennial oscillation in a) low-level meridional wind (shading, contour interval $.3 \text{ m s}^{-1}$, zero contour is omitted, but there are extra dashed contours for $-.15$ and $.15 \text{ m s}^{-1}$) and wind vectors (reference arrow = 1.5 m s^{-1}); b) surface temperature (shading, contour interval $.5 \text{ K}$) with low-level wind vectors; c) surface pressure (shading, contour interval $.1 \text{ hPa}$) with low-level wind vectors; and d) 200 hPa height (shading, contour interval $.5, 1, 1, 2 \text{ m}$) and 200 hPa wind vectors (reference arrow = 2 m s^{-1}).

Figure 10. Interannual covariance of low-level meridional wind (contour interval $.2 \text{ m s}^{-1}$, zero contour is omitted) and wind vectors (reference arrow = 1 m s^{-1}) with meridional wind at a) $42^{\circ}\text{N}, 97.5^{\circ}\text{W}$, b) $30^{\circ}\text{N}, 97.5^{\circ}\text{W}$, and c) $22^{\circ}\text{N}, 95^{\circ}\text{W}$, normalized by the interannual standard deviation of the meridional wind at the relevant reference point to give units of velocity. Confidence intervals of 99% (95%) are shaded in the dark (light) tone. (See the text for details.) Panels d-f are the same as above but with the IBO removed from all time series. Panels g-i are the same as panels d-f but for the covariance of reference-point winds with surface pressure (contour interval $.1 \text{ hPa}$) and without confidence intervals.

Figure 11. Normalized interannual covariance of monthly anomalies of low-level meridional wind (contour interval $.3 \text{ m s}^{-1}$, zero contour is omitted) and wind vectors (reference arrow = 1 m s^{-1}) with meridional wind for the Texas reference point for May through August (panels a through d, respectively). Confidence intervals of 99% (95%) are shaded in the dark (light) tone, as in Fig. 10.

Figure 12. Temporal coherence of interannual anomalies in the vicinity of the UGP reference point. Time-lag covariances between climatological anomalies of weekly-averaged low-level meridional wind (contour interval $.2 \text{ m s}^{-1}$, zero contour is omitted) and wind vectors (reference arrow = 0.5 m s^{-1}) and similar meridional wind anomalies at 42°N , 97.5°W , normalized by the standard deviation for variations of the reference point. Lag covariances progress one week per panel (left to right) from -4 weeks (panel a) to +4 weeks (panel i). Note that the contour interval is 1 m s^{-1} and the reference arrow = 1.5 m s^{-1} for the 0-week lag (panel e). Confidence intervals of 99% (95%) are shaded in the dark (light) tone, as in Fig. 10.

Figure 13. Temporal coherence of interannual anomalies in the vicinity of the Texas reference point, 30°N , 97.5°W . Similar to Fig. 12.

Figure 14. Temporal coherence of interannual anomalies in the vicinity of the Gulf reference point, 22°N , 95°W . Similar to Fig. 12.

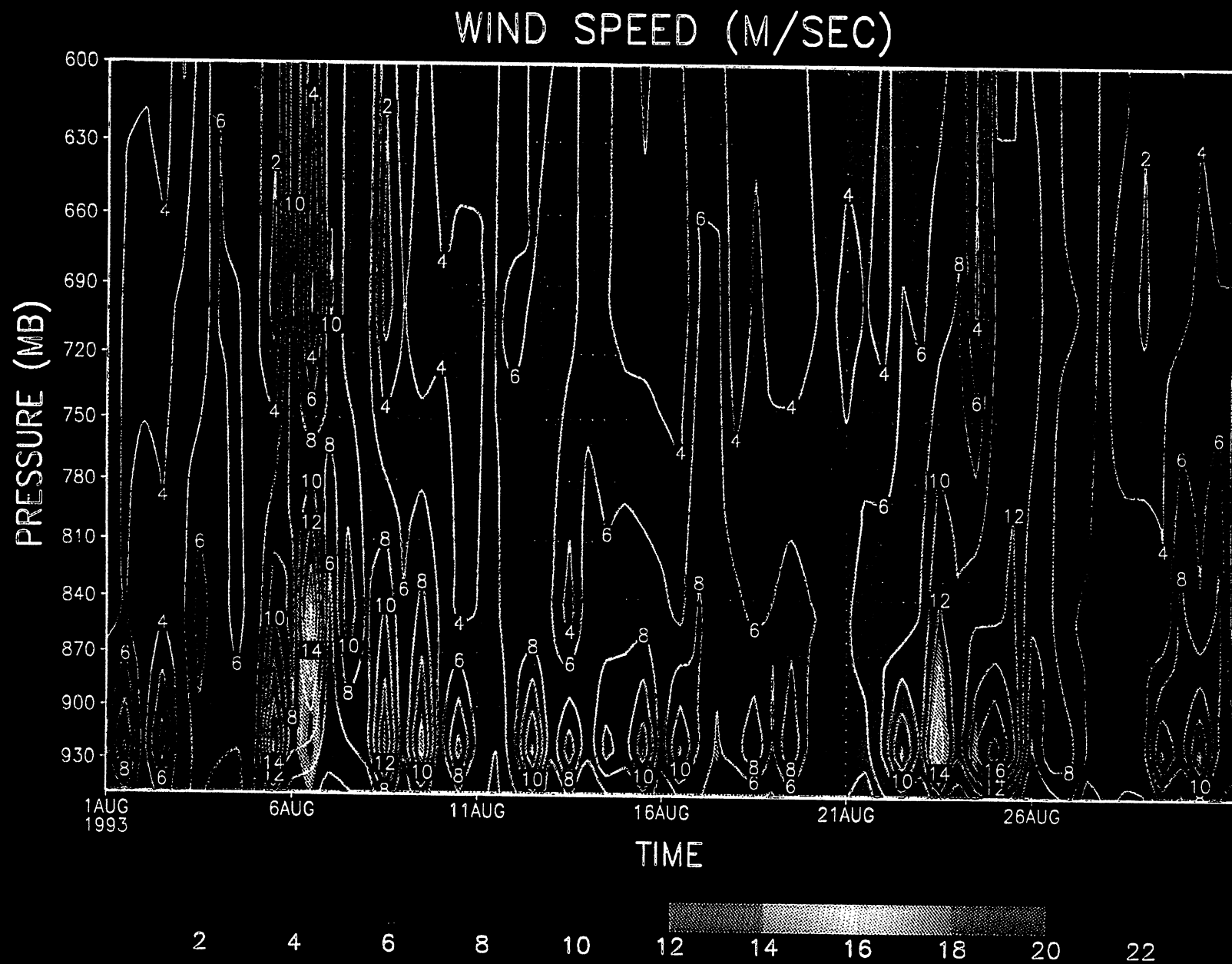


Figure 1. Time series of GPLLJ wind-speed profiles over Ft. Worth, Texas for August 1993 for an assimilation carried out with the GEOS-1 DAS with conventional data only (colored shading) and for a second validation analysis using both conventional and significant-level wind data but not the DAS (the contour lines).

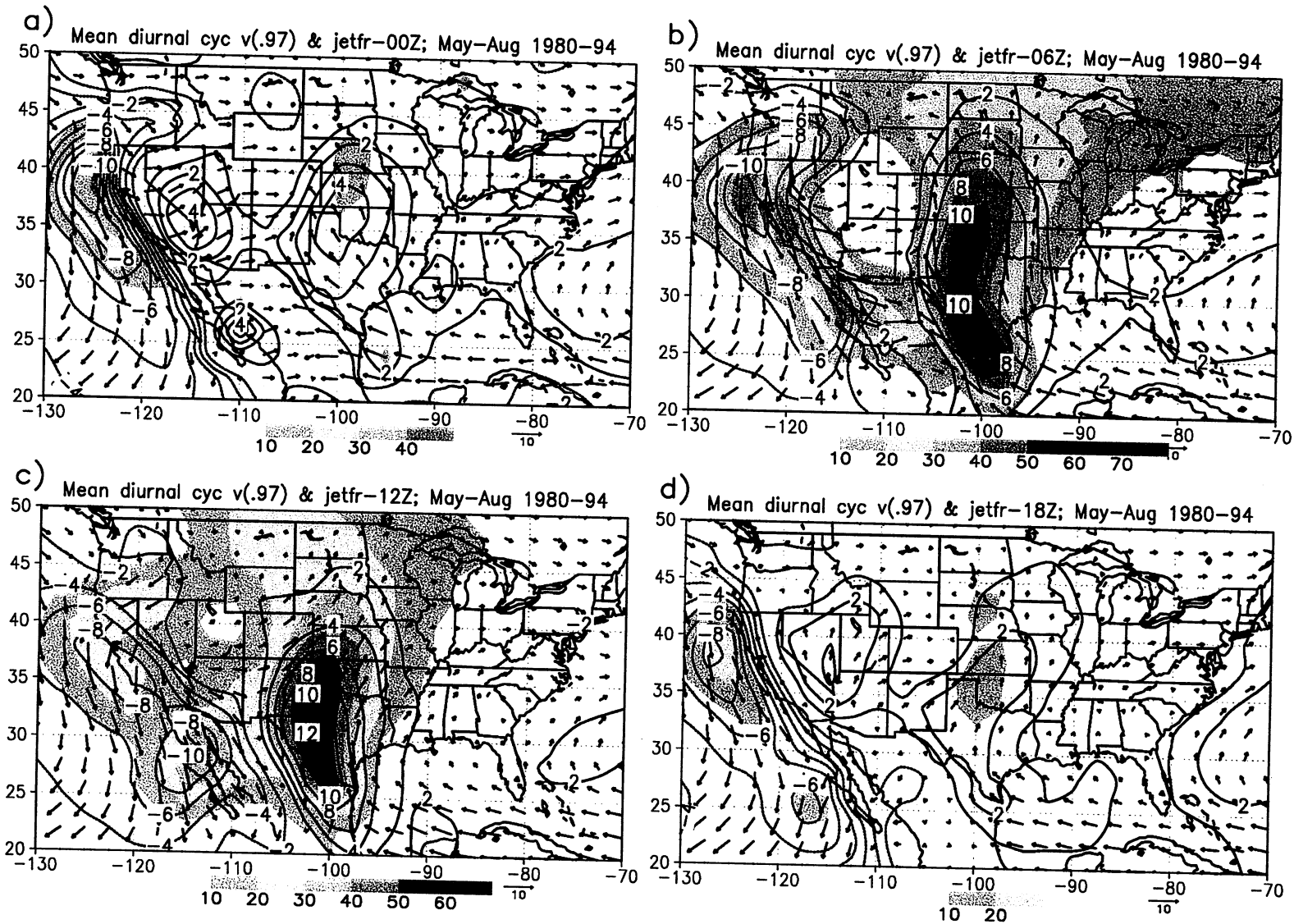


Figure 2. The mean diurnal cycle of low-level ($\sigma = .97$, about 250 m above the surface) meridional velocity (contours of 1 m s^{-1} , the zero contour is omitted), wind vectors (reference arrow = 10 m s^{-1}), and Bonner criterion-1 jet frequency (per cent, shaded). The cycle is averaged over the 15 warm seasons (May–August) of the GEOS-1 15-Year Reanalysis Data Set. Local times are a) 1800 CST, b) 0000 CST, (contours of 2 m s^{-1}), c) 0600 CST (contours of 2 m s^{-1}), and d) 1200 CST, (contours of 1 m s^{-1}), approximately 6 hours earlier than the UTC times.

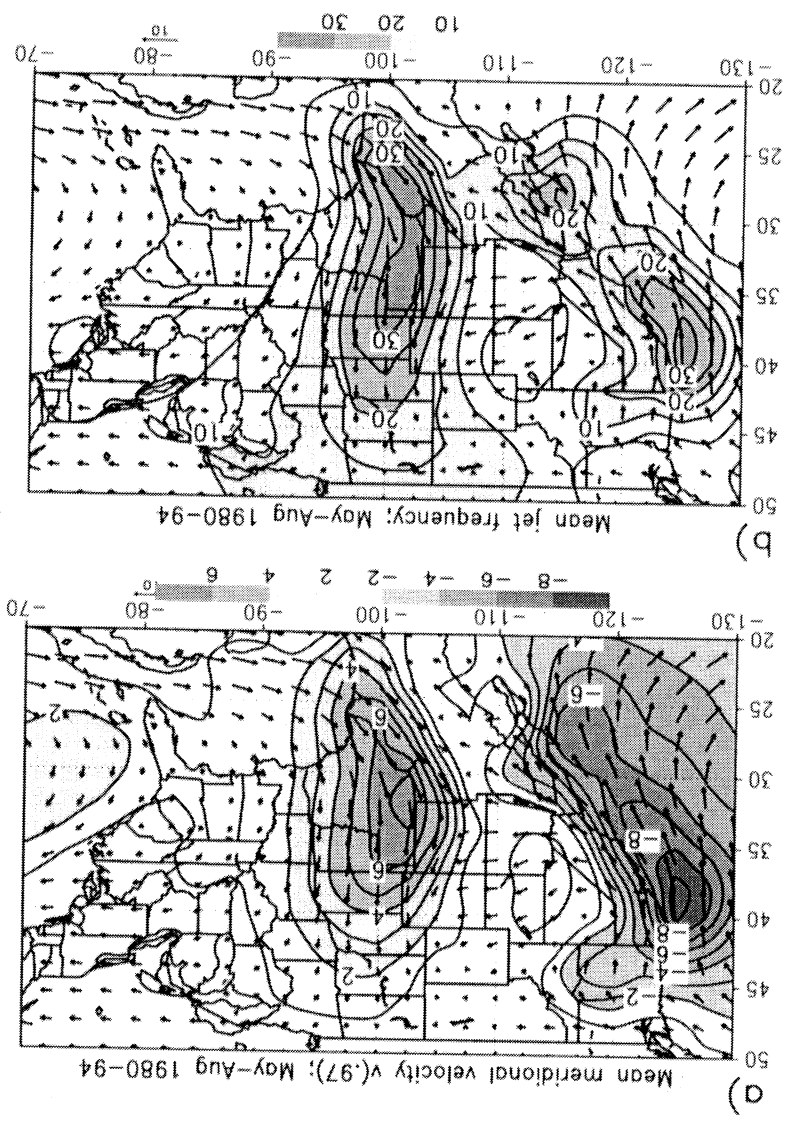


Figure 3. a) The 15-year, warm-season mean low-level wind vectors (reference arrow = 10 m s^{-1}) and low-level meridional velocity (contours of 1 m s^{-1} , the zero contour is omitted) and b) wind vectors (reference arrow = 10 m s^{-1}) and low-level meridional velocity (contours of 5 per cent) assimilated by the GEOS-1 Reanalysis Data Set.

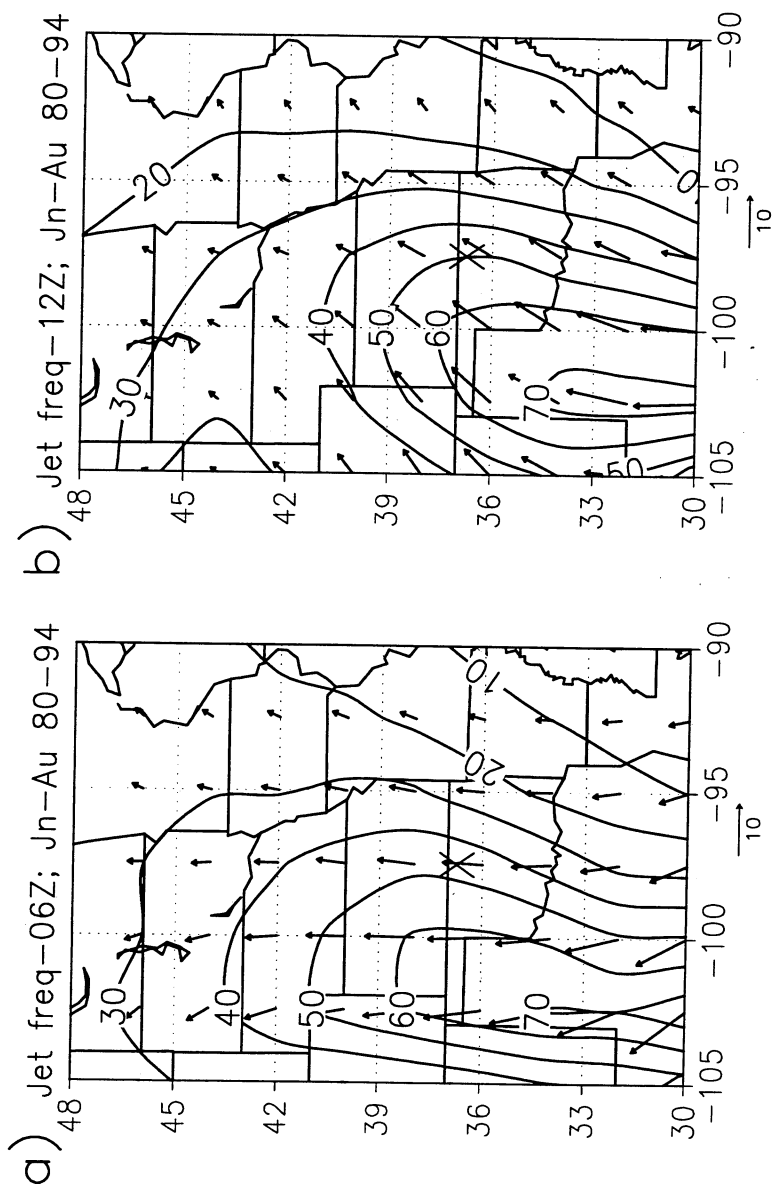


Figure 4. The 15-year, summertime (June-August) mean Bonner criterion-1 jet frequency (contours of 10 per cent) and low-level wind vectors (reference arrow = 10 m s^{-1}) assimilated by the GEOS-1 Reanalysis Data Set over the region of the NOAA Wind Profiler Network for a) 0600 UTC and b) 1200 UTC. The "X"s near the Oklahoma/Nebraska border denote the location of the ARM SGP CART site where Whiteman et al (1997) observed about 50% frequency of Bonner criterion-1 jets at both 0500 UTC and 1100 UTC.

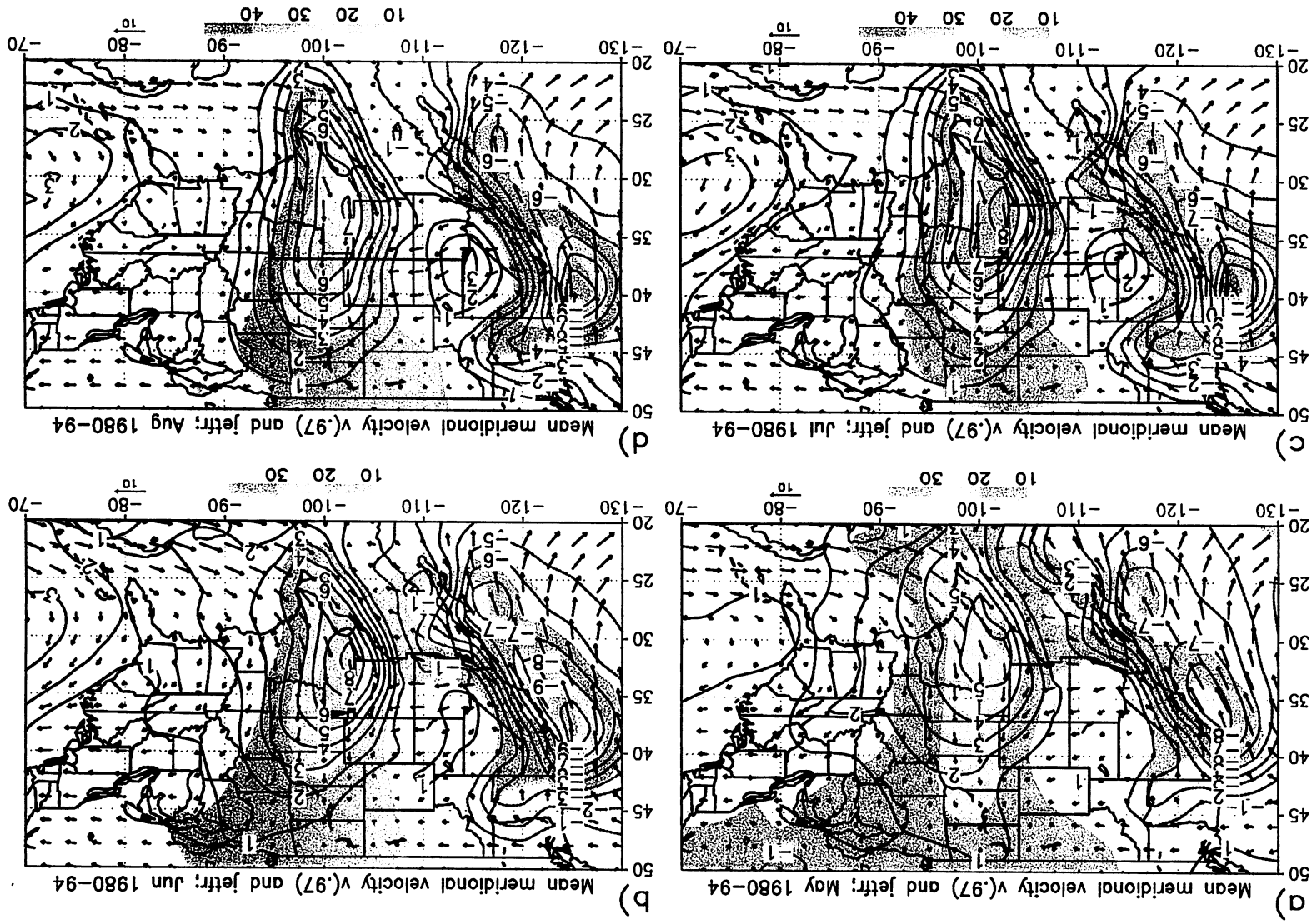


Figure 5. The mean seasonal cycle of low-level meridional velocity (contours of 1 m s⁻¹, the zero contour is omitted), wind vectors (reference arrow = 10 m s⁻¹), and Bonner criterion-1 jet frequency (per cent, shaded) during the warm season May-August. The cycle is averaged over the 15-year period of the GEOS-1 Reanalysis Data Set.

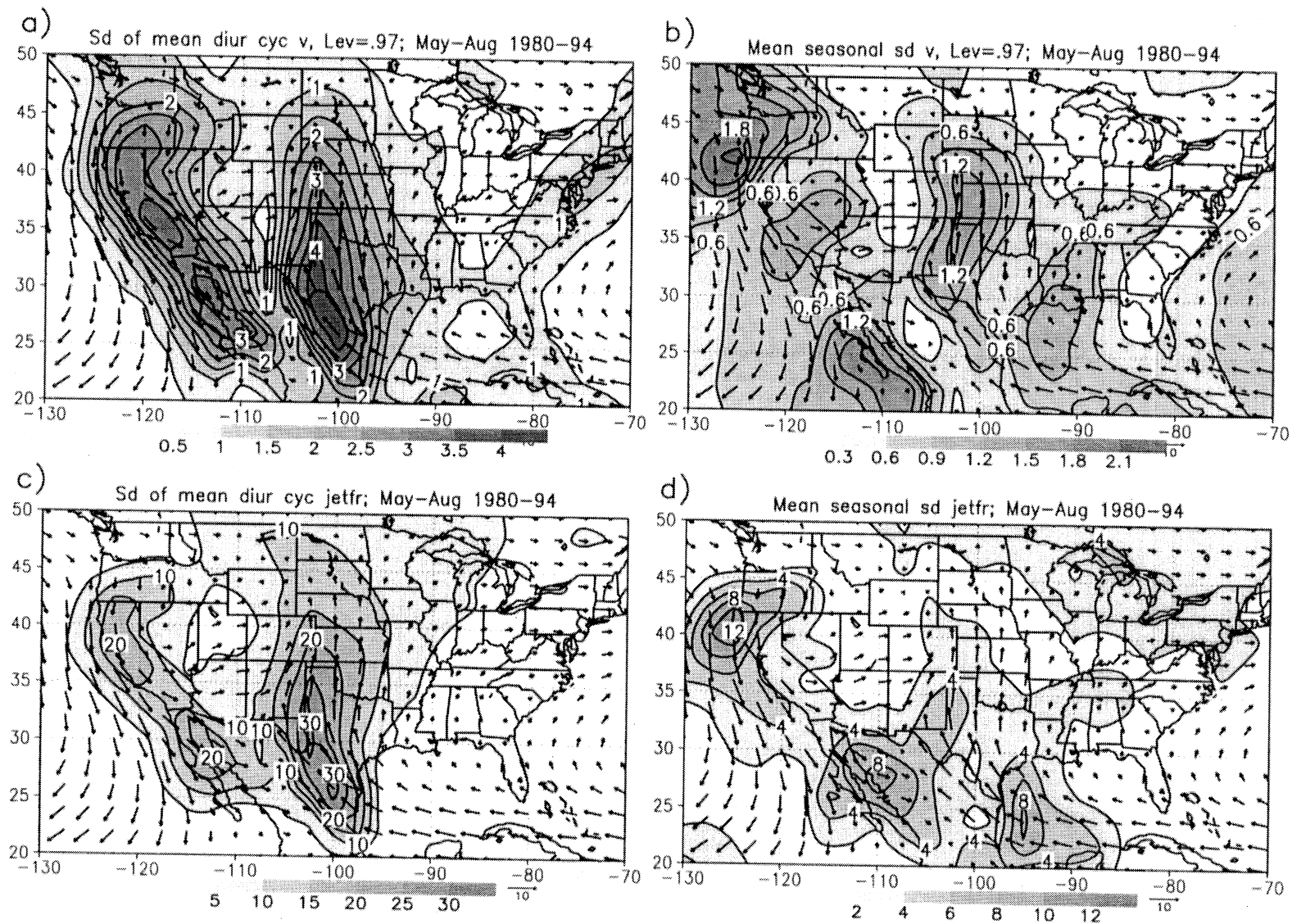


Figure 6. Standard deviation of the mean diurnal cycle of Fig. 2 (panels a and c), and the mean seasonal cycle of Fig. 4 (panels b and d). Low-level meridional wind (shaded, contour interval .25, .15 m s⁻¹) is shown in panels a and b and Bonner criterion 1 jet frequency (shaded, contour interval 5, 2 per cent) is shown in panels c and d. These are superimposed over the 15-year, warm-season mean low-level wind vectors (reference arrow = 10 m s⁻¹).

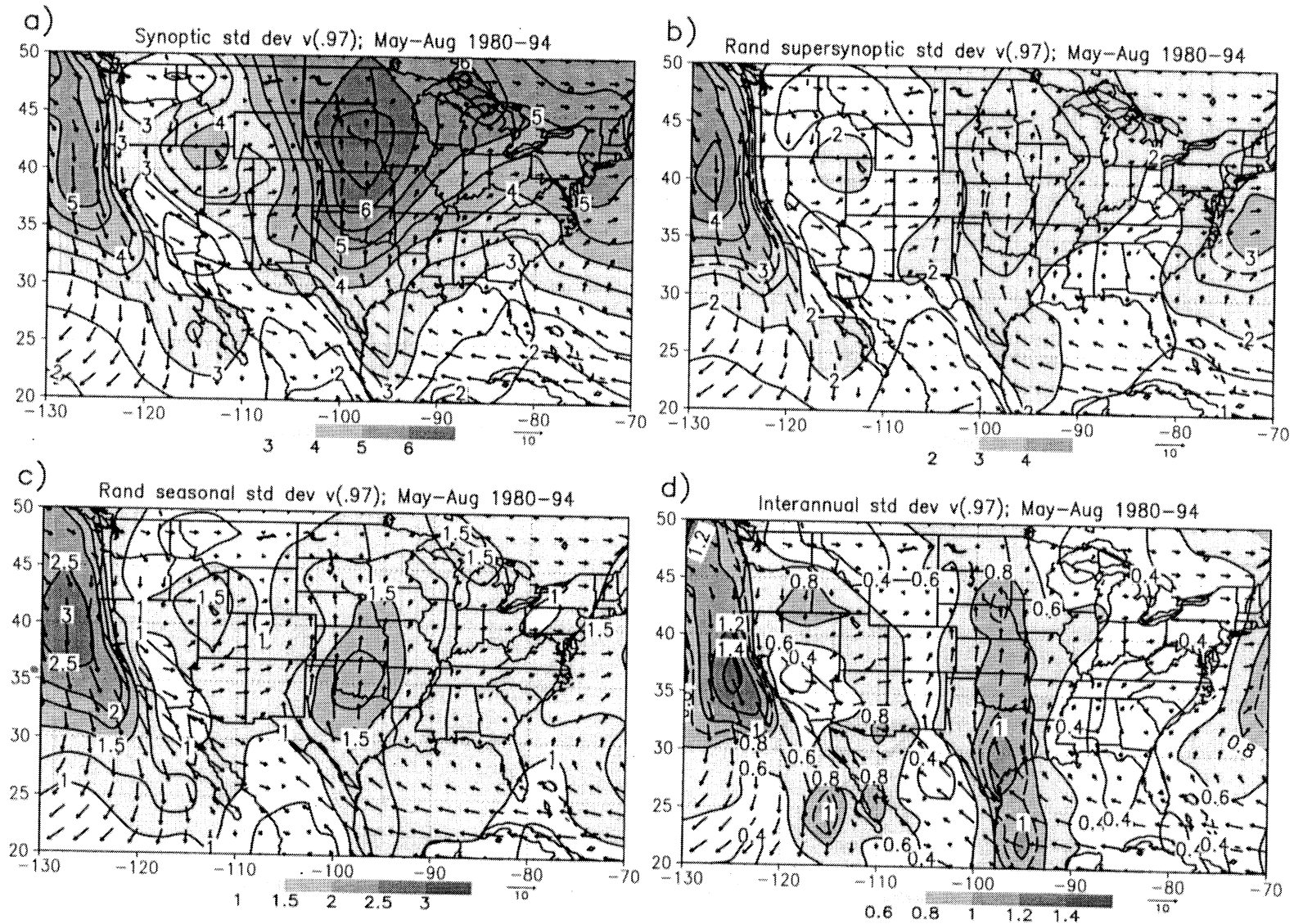
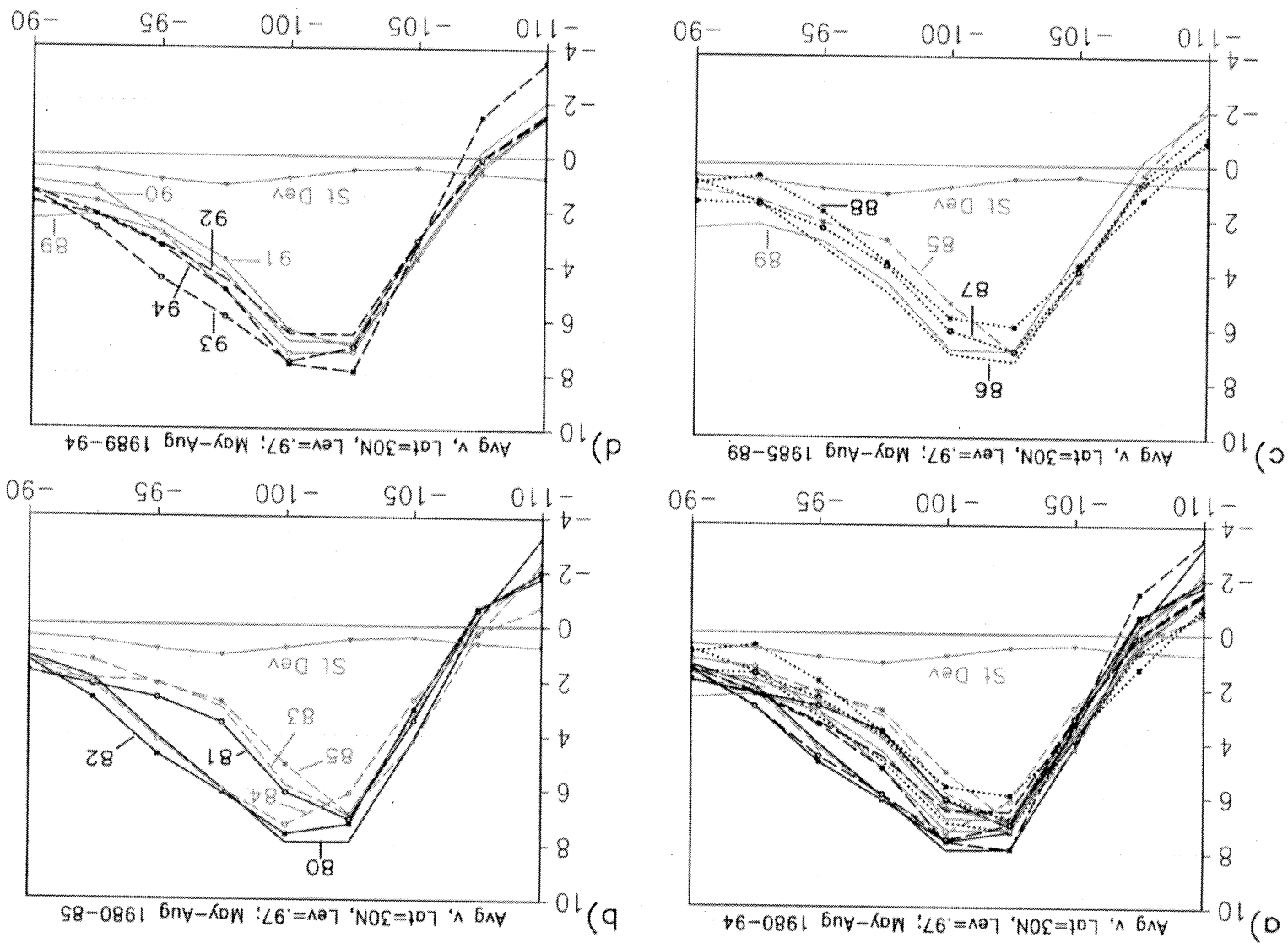


Figure 7. Standard deviation of low-level meridional velocity (shaded, contour interval $.5 \text{ m s}^{-1}$) associated with natural, random variability on a) the synoptic time scale (more than a day and up to 8 days), b) the super-synoptic time scale (more than 8 days and up to a month, with the mean seasonal cycle removed, with an extra dashed contour for 2.75 m s^{-1}), c) the seasonal time scale (more than a month and up to a season, with the mean seasonal cycle removed, contour interval $.25 \text{ m s}^{-1}$), and d) the interannual time scale (warm-season averages, contour interval $.1 \text{ m s}^{-1}$ with an extra dashed contour for 0.9 m s^{-1}). Vectors are mean low-level flow (reference arrow = 10 m s^{-1}).

Figure 8. Cross-sections of the mean low-level meridional velocity (ms^{-1}) at 30°N latitude a) for each of the 15 warm seasons of the GEOS-1 Reanalysis Data Set with the interannual standard deviation in the gray line with triangles and b-d) repeated, 5 or 6 at a time, with the same sequence of colors, line styles (solid, dashed, or dotted), and line markings (no markings, open circles or closed squares) and labeled by year. Notice the marked biennial oscillation of the profiles during the first 6 years (1980-85) of the data set (panel b).



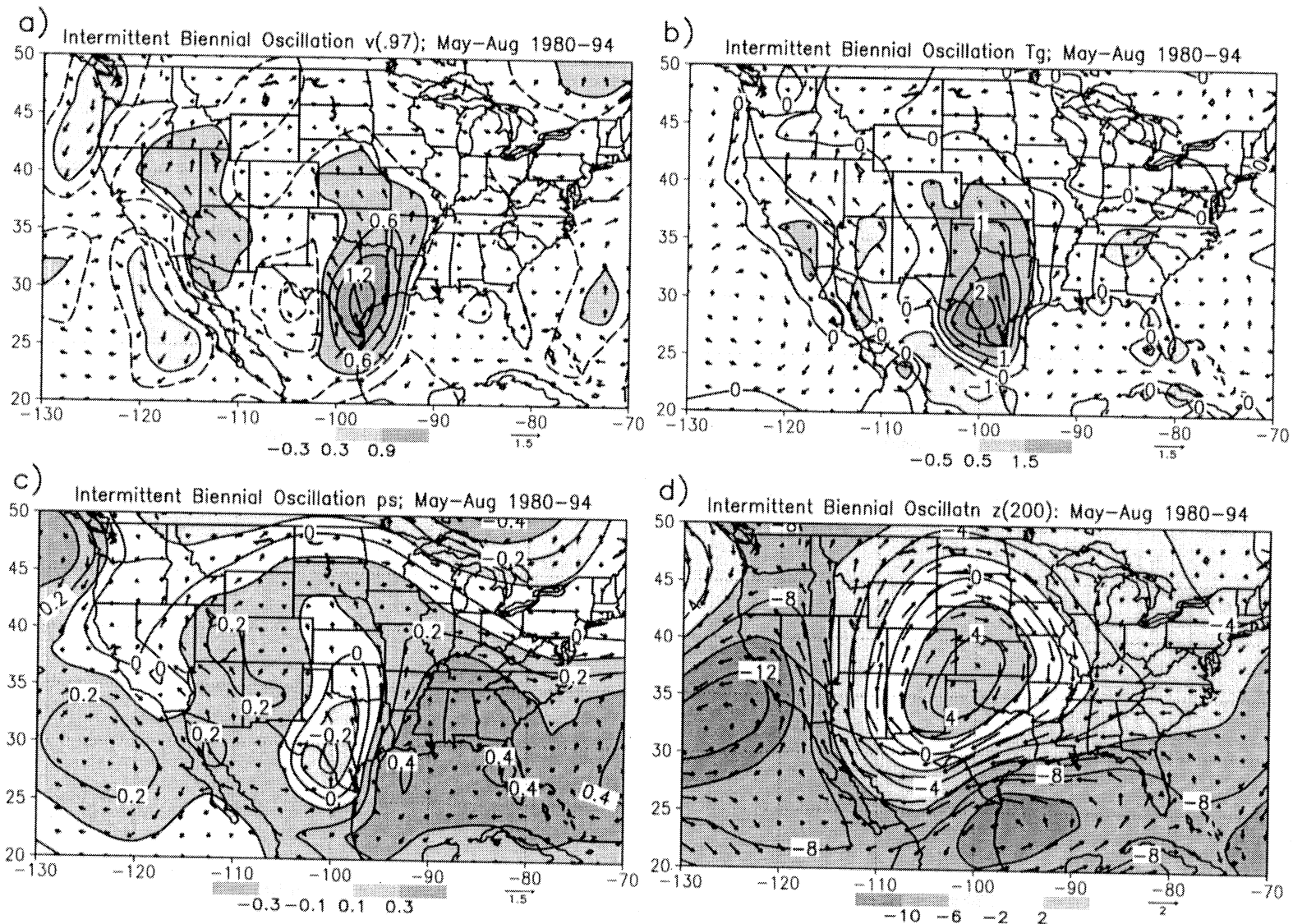


Figure 9. The intermittent biennial oscillation in a) low-level meridional wind (shading, contour interval $.3 \text{ m s}^{-1}$, zero contour is omitted, but there are extra dashed contours for $-.15$ and $.15 \text{ m s}^{-1}$) and wind vectors (reference arrow = 1.5 m s^{-1}); b) surface temperature (shading, contour interval $.5 \text{ K}$) with low-level wind vectors; c) surface pressure (shading, contour interval $.1 \text{ hPa}$) with low-level wind vectors; and d) 200 hPa height (shading, contour interval $.5, 1, 1, 2 \text{ m}$) and 200 hPa wind vectors (reference arrow = 2 m s^{-1}).

Figure 10. Interannual covariance of low-level meridional wind (contour interval 2 m s^{-1} , zero contour is omitted) and wind vectors (reference arrow = 1 m s^{-1}) with meridional wind at the relevant reference point to give units of velocity. Confidence intervals of 99% (95%) are shaded in the dark (light) tone. (See the text for details.) Panels d-f are the same as above but with the IBO removed from all time series. Panels g-i are the same as panels d-f but for the covariance of reference-point winds with surface pressure (contour interval 1 hPa) and without confidence intervals.

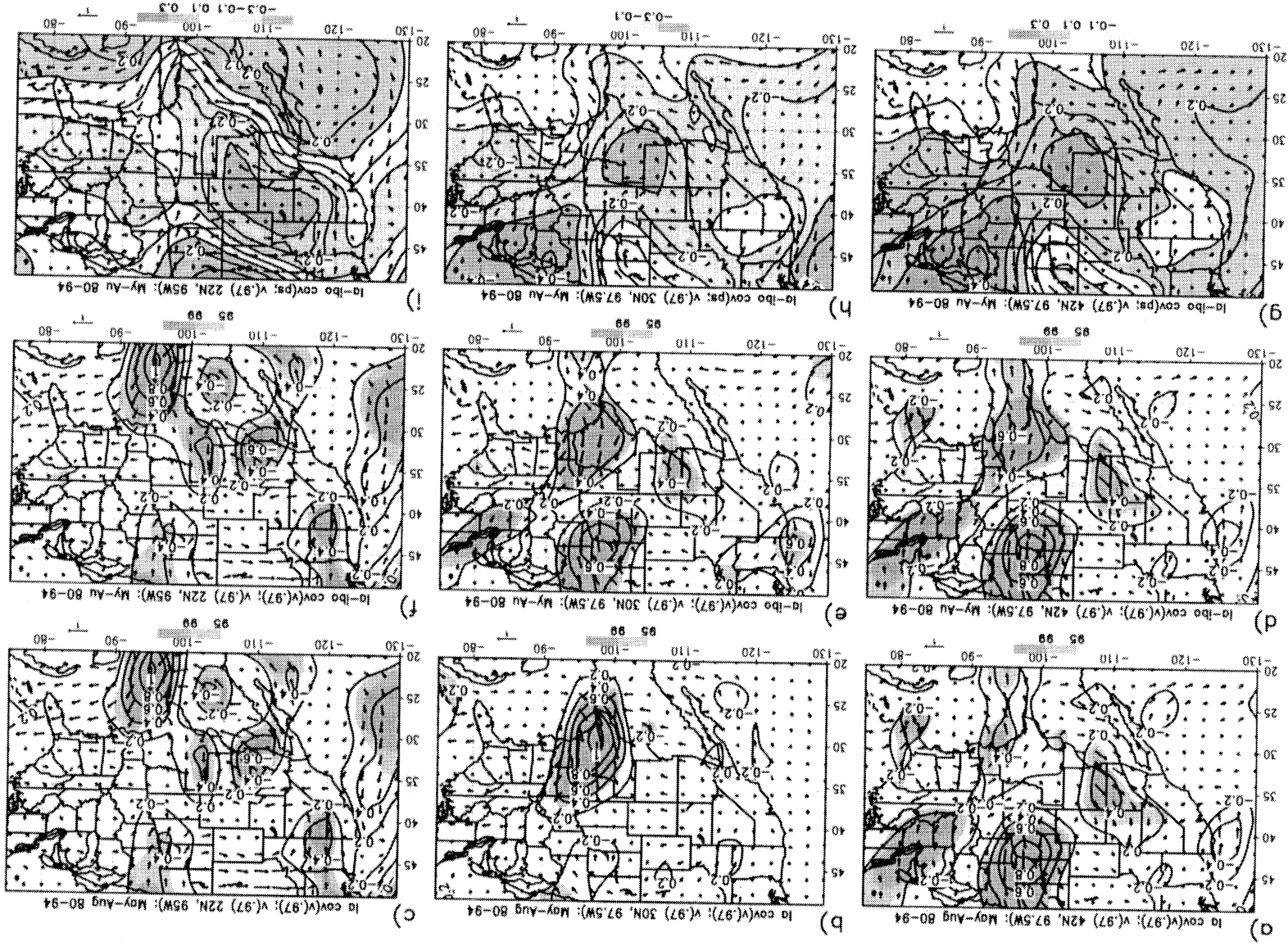
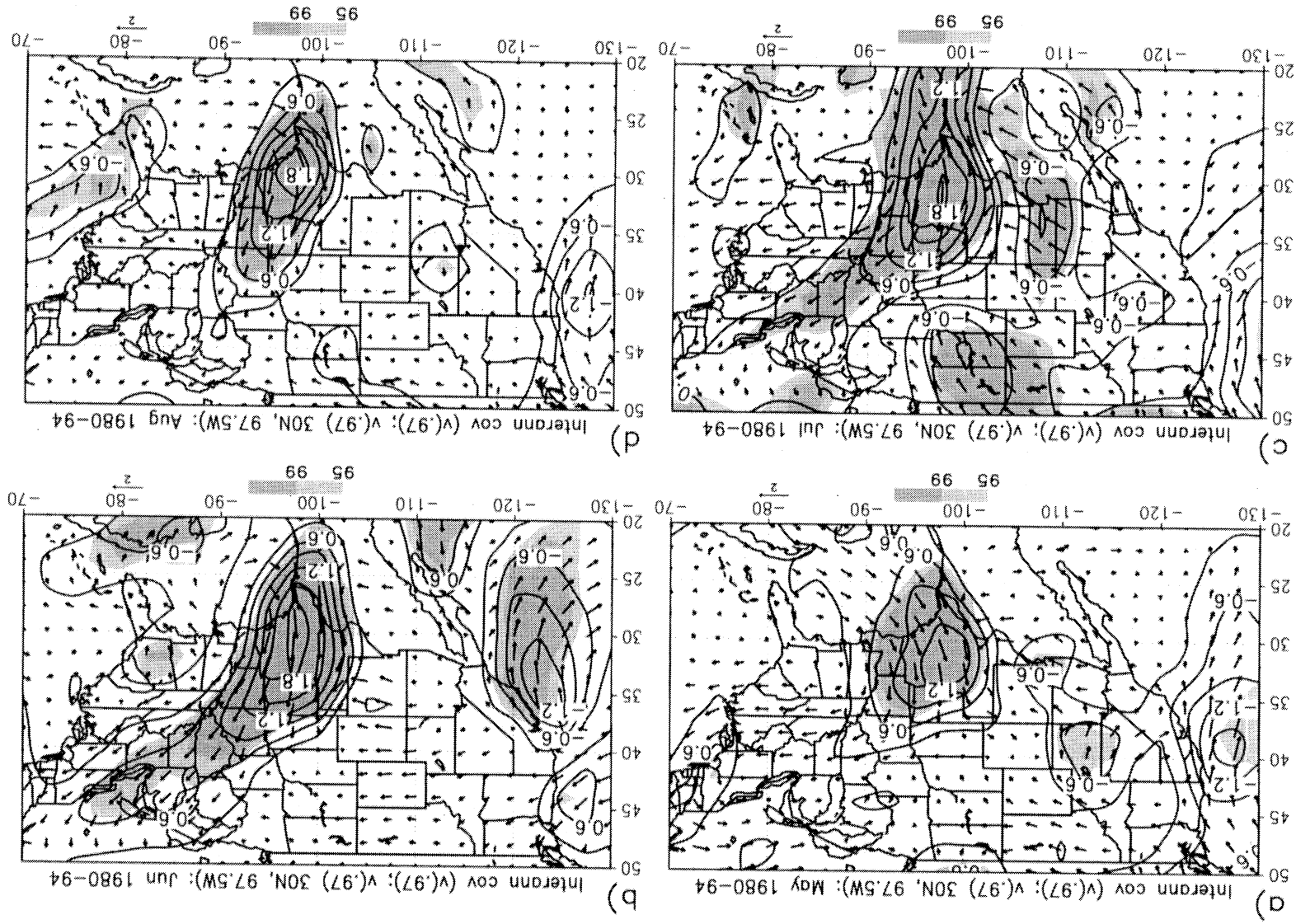


Figure 11. Normalized interannual covariance of monthly anomalies of low-level meridional wind (contour interval $.3 \text{ m s}^{-1}$, zero contour is omitted) and wind vectors (reference arrow = 1 m s^{-1}) with meridional wind (reference point for May through August (panels a through d, respectively). Confidence intervals of 99% (95%) are shaded in the dark (light) tone, as in Fig. 10.



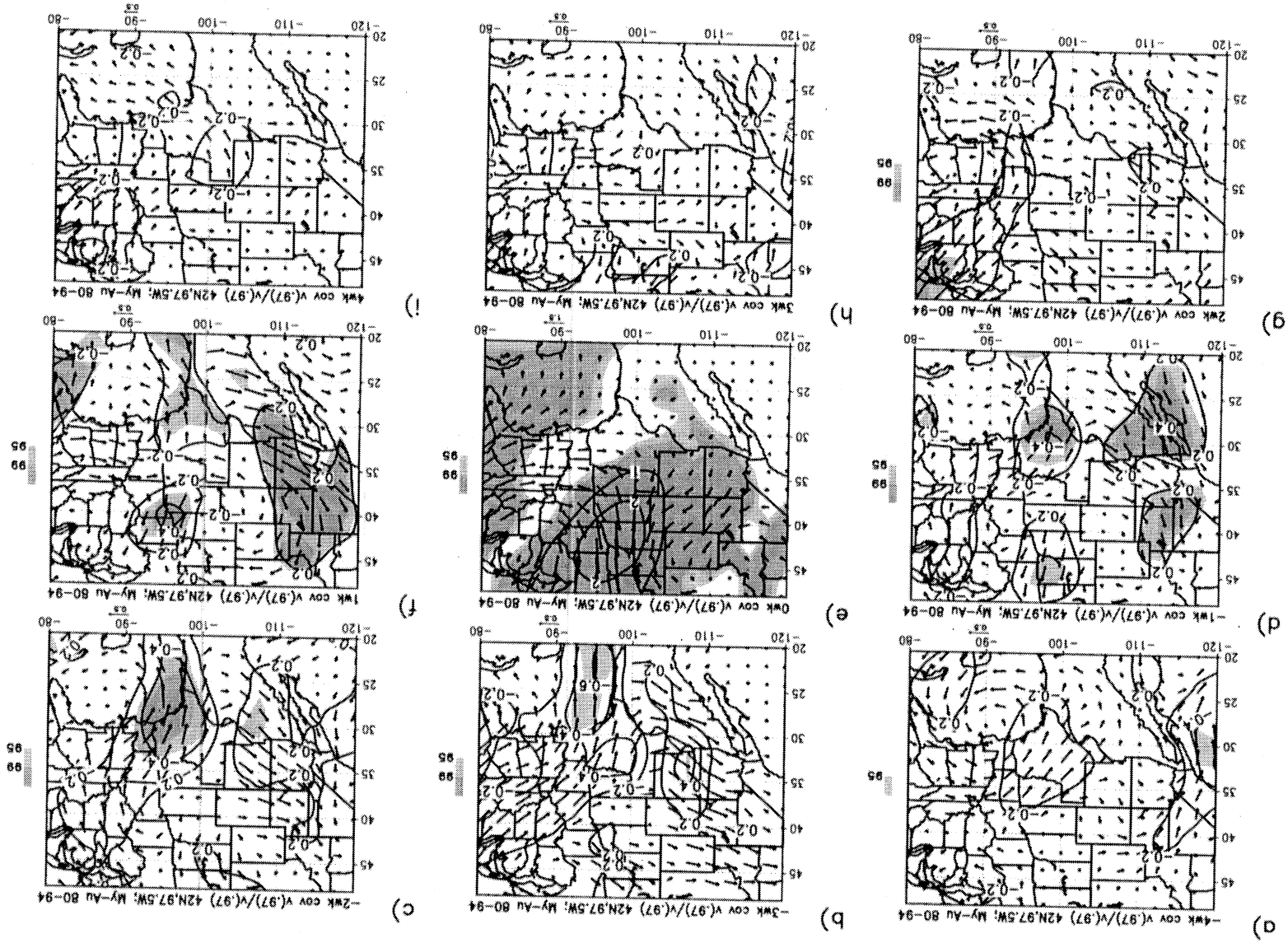
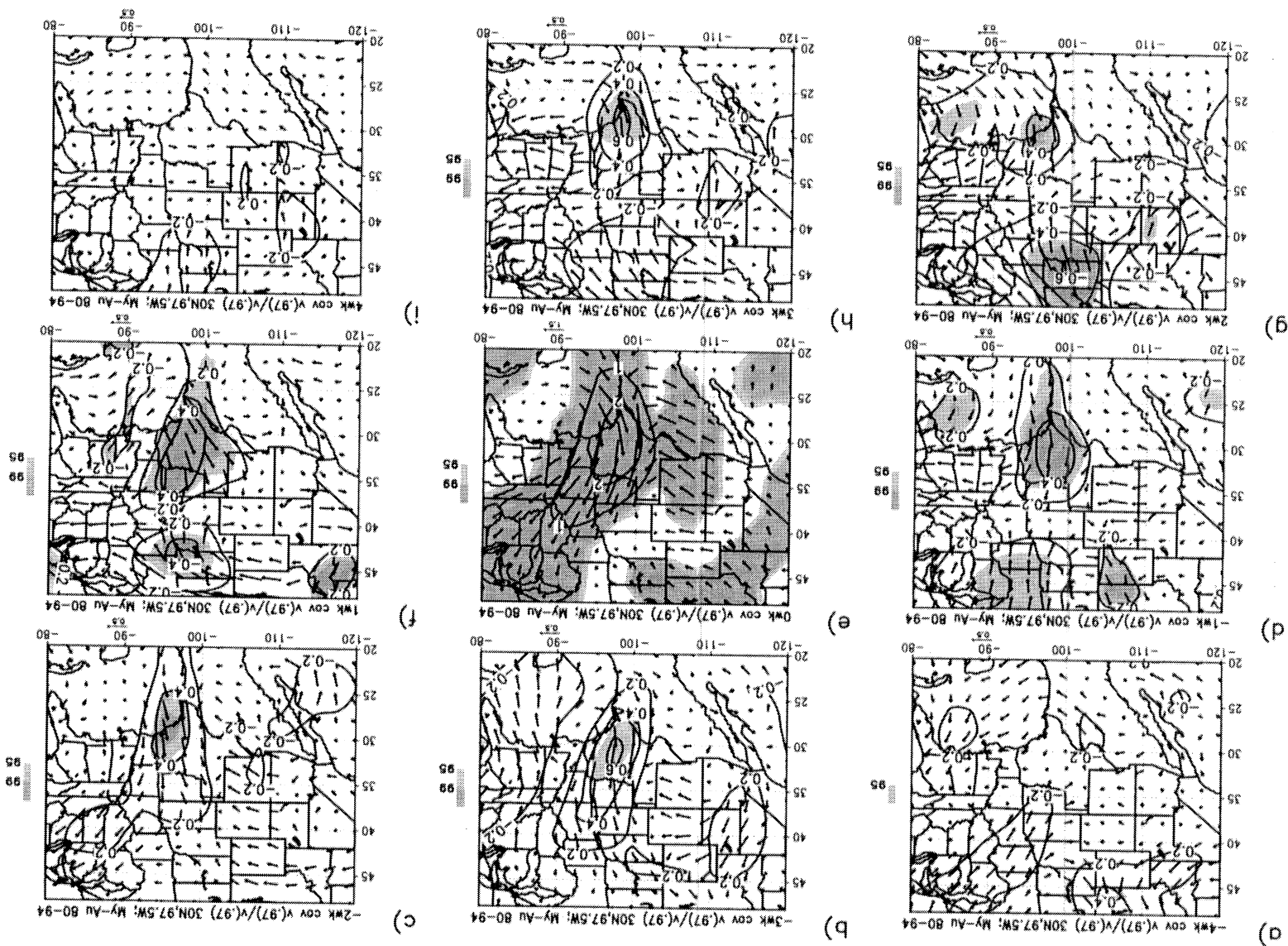


Figure 12. Temporal coherence of interannual anomalies in the vicinity of the UGP reference point. Time-lag covariances between vectors (reference arrow = 0.5 m s⁻¹) and similar meridional wind (contour interval 2 m s⁻¹, zero contour is omitted) and wind variations of the reference point. Lag covariances progress one week per panel (left to right) from -4 weeks (panel a) to +4 weeks (panel i). Note that the contour interval is 1 m s⁻¹ and the reference arrow = 1.5 m s⁻¹ for the 0-week lag (panel e). Confidence intervals of 99% (95%) are shaded in the dark (light) tone, as in Fig. 10.

Figure 13. Temporal coherence of interannual anomalies in the vicinity of the Texas reference point, 30°N, 97.5°W. Similar to Fig. 12.



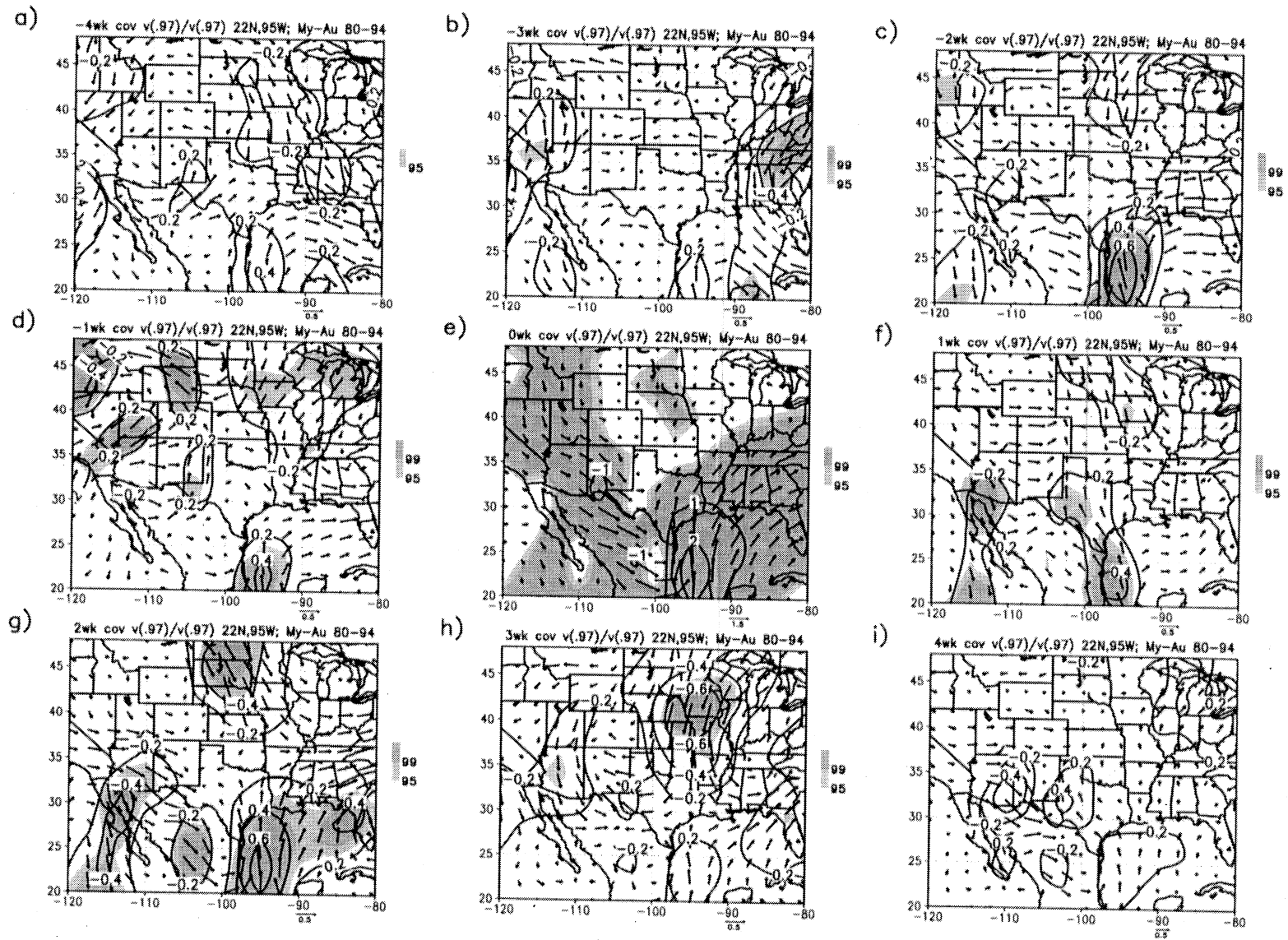


Figure 14. Temporal coherence of interannual anomalies in the vicinity of the Gulf reference point, 22°N , 95°W . Similar to Fig. 12.